PCCP

ROYAL SOCIETY OF CHEMISTRY

PERSPECTIVE

View Article Online
View Journal | View Issue

Cite this: *Phys. Chem. Chem. Phys.*, 2022, **24**, 17397

The evolution of paramagnetic NMR as a tool in structural biology

Enrico Ravera, [abc] Lucia Gigli, [abc] Letizia Fiorucci, [abc] Claudio Luchinat [abc] and Giacomo Parigi *[abc]

Paramagnetic NMR data contain extremely accurate long-range information on metalloprotein structures and, when used in the frame of integrative structural biology approaches, they allow for the retrieval of structural details to a resolution that is not achievable using other techniques. Paramagnetic data thus represent an extremely powerful tool to refine protein models in solution, especially when coupled to X-ray or cryoelectron microscopy data, to monitor the formation of complexes and determine the relative arrangements of their components, and to highlight the presence of conformational heterogeneity. More recently, theoretical and computational advancements in quantum chemical calculations of paramagnetic NMR observables are progressively opening new routes in structural biology, because they allow for the determination of the structure within the coordination sphere of the metal center, thus acting as a loupe on sites that are difficult to observe but very important for protein function.

Received 21st April 2022,
Accepted 28th June 2022

DOI: 10.1039/d2cp01838a

rsc.li/pccp

Introduction

NMR spectroscopy has long proven a powerful technique for determining the structure of biological macromolecules. X-ray diffraction structures account for 87% of the protein data bank (PDB), and to date, the number of electron microscopy and NMR structures has become comparable (5.6% *vs.* 7.2%). However, X-ray and cryo-electron microscopy require crystallization and rapid freeze treatment, respectively, whereas NMR is performed in solution or on sedimented samples and thus has the advantage to operate at higher temperatures and in close to biologically relevant conditions.[1] Furthermore, NMR remains the method of choice for the investigation of dynamics. The presence of a paramagnetic metal ion can provide an additional source of valuable information, at a level that is often hardly accessible with other techniques: paramagnetic centers affect the NMR spectra of proteins in ways that depend (besides on the type of paramagnetic metal) on the fine (sub-Å) detail of the coordination environment of the metal ion and of the distribution of protein nuclei, even if these are nanometers away from the metal.

The major paramagnetic NMR effects, due to the dipole–dipole interaction between nuclear and electron magnetic moments, are the changes with respect to the values measured for an analogue diamagnetic system in (i) nuclear relaxation rates, called paramagnetic relaxation enhancements (PREs), (ii) NMR shifts of the protein nuclei, called hyperfine shifts, and (iii) coupling constants between paired nuclei, called paramagnetic residual dipolar couplings (pRDCs). Hyperfine shifts are composed of pseudocontact shifts (PCSs) and, in the presence of unpaired electron spin density onto the observed nuclei, Fermi-contact shifts (FCSs). All these paramagnetic effects report on the structural details of the protein and on the variability thereof in the NMR time scale and are thus increasingly used as structural restraints.

The obtainment of the paramagnetic NMR restraints depends critically on the electronic structure of the paramagnetic center; they are in general measured as the difference of a given observable for the same protein with and without the paramagnetic metal that can be (i) replaced by a diamagnetic metal ion, (ii) reduced to a diamagnetic state, or (iii) removed from the protein.

The first protein structure calculations taking advantage of paramagnetic NMR restraints date back to the nineties. PREs were included in solution structure protocols in the first solution structures of paramagnetic proteins.[2] The introduction of PCSs in structural determination was demonstrated in 1996,[3] and shortly afterwards pRDCs were introduced.[4,5] These two classes of restraints, combined with paramagnetic cross-correlated relaxation rates,[6,7] allowed us to obtain the first backbone structure

[a] *Magnetic Resonance Center (CERM), University of Florence, via Luigi Sacconi 6, Sesto Fiorentino, 50019, Italy*
[b] *Department of Chemistry "Ugo Schiff", University of Florence, via della Lastruccia 3, Sesto Fiorentino, 50019, Italy*
[c] *Consorzio Interuniversitario Risonanze Magnetiche Metallo Proteine (CIRMMP), via Luigi Sacconi 6, Sesto Fiorentino, 50019, Italy. E-mail: parigi@cerm.unifi.it*

of a protein only relying on paramagnetic restraints.[8,9] Also PREs measured through tailored experiments even for nuclei close to the paramagnetic center could be used to determine the structure of a small protein.[10] These examples show the importance and the relevance of the structural information contained in these restraints. When dealing with paramagnetic proteins, paramagnetic NMR restraints should thus be always included in protein structure calculation protocols together with all other available restraints, mainly distance restraints determined from NOEs (nuclear Overhauser effects) and dihedral angle restraints from NMR chemical shifts.

Important advances have been made in the last few years regarding the protein structure refinement strategies through paramagnetic data, the theory of paramagnetic NMR shift and relaxation, the calculation from first-principles of quantum mechanics of hyperfine shifts, and the implementation of tools for their use as structural restraints. Some of the main achievements will be discussed in the following sections in light of the new perspectives they are disclosing.

The electron–nucleus interaction: the origin of relaxation and shift

The electron–nucleus or hyperfine interaction can be divided into two contributions, one arising from the interaction of the nuclear magnetic moment with the unpaired electron spin density (ρ_I) residing on it (called Fermi-contact interaction) and due to both direct electron spin delocalization and spin polarization, and another arising from the through-space interaction of the nuclear magnetic moment with the electron magnetic moment (called dipolar interaction).[11,12] This second term comprises the nuclear spin–electron spin interaction as well as the interaction between the nuclear spin and the electron orbital magnetic moment.[13,14]

Given that electron relaxation occurs orders of magnitude faster than nuclear relaxation, the nucleus senses fluctuating fields originating from the hyperfine interaction, and further nuclear spin relaxation mechanisms become available (PRE, *vide infra*). Because in the presence of a magnetic field, the electron spin magnetic moment (for Fermi-contact interaction) and the overall electron magnetic moment (for dipolar interaction) are not null due to the different population of the electronic states, the nuclear resonances shifted (hyperfine shift, *vide infra*).

The paramagnetic relaxation enhancements

Nuclear relaxation rates in paramagnetic metalloproteins depend on several relaxation mechanisms all related to the presence of the paramagnetic center which add to the diamagnetic relaxation rates. One relaxation mechanism depends on the modulation of the dipole coupling with the electron spin according to the Solomon equations:[15]

$$R_{1M}^{dip} = \frac{2}{15}\left(\frac{\mu_0}{4\pi}\frac{\gamma_I g_{iso}\mu_B}{r^3}\right)^2 S(S+1)\left[\frac{7\tau_{c2}^{dip}}{1+\omega_s^2\left(\tau_{c2}^{dip}\right)^2}+\frac{3\tau_{c1}^{dip}}{1+\omega_I^2\left(\tau_{c1}^{dip}\right)^2}\right] \quad (1a)$$

$$R_{2M}^{dip} = \frac{1}{15}\left(\frac{\mu_0}{4\pi}\frac{\gamma_I g_{iso}\mu_B}{r^3}\right)^2 S(S+1) \times \left[4\tau_{c1}^{dip}+\frac{13\tau_{c2}^{dip}}{1+\omega_s^2\left(\tau_{c2}^{dip}\right)^2}+\frac{3\tau_{c1}^{dip}}{1+\omega_I^2\left(\tau_{c1}^{dip}\right)^2}\right] \quad (1b)$$

$$\left(\tau_{ci}^{dip}\right)^{-1} = \tau_r^{-1} + \tau_{ei}^{-1}$$

where τ_r and τ_{ei} are the reorientation time and the longitudinal (i = 1) and transverse (i = 2) electron relaxation times, respectively. In the case of lanthanoids and actinoids, the J quantum number substitutes the S quantum number and g_J substitutes g_{iso}. These equations are derived from a number of assumptions, which include (but are not limited to): (i) the point-dipole approximation for the electron spin, (ii) isotropic molecular reorientations, (iii) isotropic **g** tensors and an electron Zeeman interaction much larger, at the field of interest, than zero-field splitting (ZFS), and hyperfine coupling between the electron spin and metal nuclear spin (for paramagnetic metals with $I > 0$). Recent experimental works have shown that in some cases these assumptions cannot be safely made even at high magnetic fields, and tools for managing experimental data have been proposed (see later).

When electron relaxation times are very short, nuclear relaxation caused by the Solomon equations is modest, and significant contributions to nuclear relaxation can arise from the modulation of the dipole–dipole interaction between the nuclear magnetic moment and the averaged electron magnetic moment (*Curie spin relaxation*). This contribution depends on the molecular reorientation time and on the magnetic susceptibility, and, in the case of isotropic χ tensors, Curie spin PREs are given by:[16]

$$R_{1M}^{CS} = \frac{2}{5(4\pi)^2}\frac{\omega_I^2\chi^2}{r^6}\frac{3\tau_r}{1+\omega_I^2\tau_r^2} \quad (2a)$$

$$R_{2M}^{CS} = \frac{1}{5(4\pi)^2}\frac{\omega_I^2\chi^2}{r^6}\left[4\tau_r+\frac{3\tau_r}{1+\omega_I^2\tau_r^2}\right] \quad (2b)$$

For paramagnetic transition metal ions and for gadolinium(III), when excited states are far from the ground state, $\chi = \frac{\mu_0\mu_B^2 g_e^2 S(S+1)}{3kT}$ (spin-only approximation). In lanthanoids, because the spin–orbit coupling energy is generally larger than the effect of the crystal field, S is substituted by the spin–orbit coupled quantum number J, g_e by the Landé g-factor g_J, and the isotropic χ becomes $\chi = \frac{\mu_0\mu_B^2 g_J^2 J(J+1)}{3kT}$.

The anisotropy of χ affects the Curie spin PREs,[17] which can be calculated, as recently shown,[18] with the following expression:

$$R_{1M}^{CS} = \frac{1}{2}\Delta_\sigma^2\omega_I^2\frac{\tau_r}{1+9\omega_I^2\tau_r^2}+\frac{2}{15}\Delta_\sigma^2\omega_I^2\frac{\tau_r}{1+\omega_I^2\tau_r^2} \quad (3a)$$

$$R_{2M}^{CS} = \frac{1}{4}\Delta_\sigma^2\omega_I^2\frac{\tau_r}{1+9\omega_I^2\tau_r^2}+\frac{1}{45}\Delta_\sigma^2\omega_I^2\left[4\tau_r+\frac{3\tau_r}{1+\omega_I^2\tau_r^2}\right] \quad (3b)$$

with

$$\Delta_\sigma^2 = (\sigma_{xy} - \sigma_{yx})^2 + (\sigma_{xz} - \sigma_{zx})^2 + (\sigma_{yz} - \sigma_{zy})^2$$

$$\Delta_\sigma^2 = \sigma_{xx}^2 + \sigma_{yy}^2 + \sigma_{zz}^2 - \sigma_{xx}\sigma_{yy} - \sigma_{xx}\sigma_{zz} - \sigma_{yy}\sigma_{zz} + \frac{3}{4}\left[(\sigma_{xy} + \sigma_{yx})^2 + (\sigma_{xz} + \sigma_{zx})^2 + (\sigma_{yz} + \sigma_{zy})^2\right]$$

where $\boldsymbol{\sigma}$ is the dipolar shielding tensor:

$$\boldsymbol{\sigma} = -\frac{1}{4\pi r^3}\boldsymbol{\chi} \cdot \left(\frac{3\mathbf{r}\mathbf{r}^T}{r^2} - \mathbf{1}\right), \quad (4)$$

and the isotropic average of which corresponds to the PCS δ^{pc} (see below eqn (5)).

As already indicated, eqn (1) for PREs is derived from the isotropic **g** tensor and from the absence of ZFS and hyperfine coupling between unpaired electron(s) and metal nuclear magnetic moment. The latter effects can significantly affect the energy of electronic spin transitions, in such a way that sizably different rates are calculated, depending, for instance, on the magnitude of the ZFS energy with respect to the Zeeman energy, as well as on the position of the nucleus with respect to the axes of the ZFS tensor, with origin on the metal ion. Therefore, for systems with large ZFS, PREs have a structural dependence not limited to the metal–nuclear distance (as in eqn (1)), but comprising also the spherical angles defining the metal–nucleus direction in the ZFS frame.[19–22]

The evidence of the angular dependence of PREs has been obtained experimentally for a paramagnetic lanthanoid(III) complex with a large static ZFS.[18] PRE data, measured at 1 T, could in fact not be satisfactorily fitted using the Solomon equation (eqn (1a)) and showed a dependence on the direction of the **r** vector. PRE values were found to correlate with the sign of the PCSs, and thus to depend on the sign and orientation of the $\boldsymbol{\Delta\chi}$ tensor, and could be nicely fitted using the parametric equation:

$$R_{1M}^{dip} = \frac{2}{3}\left(\frac{\mu_0}{4\pi}\right)^2 \frac{\gamma_I^2}{r^6} \mathrm{Tr}\left[\left(\frac{3\mathbf{r}\mathbf{r}^T}{r^2} - \mathbf{1}\right)^2 \mathbf{G}(\omega_I)\right]$$

where the six independent components of the symmetric spectral density tensor $\mathbf{G}(\omega_I)$ are treated as fitting parameters. The angular dependence of PREs is thus ascribed to the effect of the ZFS energy much larger than the electron Zeeman energy, as the Curie contribution and the effect of the magnetic susceptibility anisotropy on it (eqn (3a)) were calculated to be negligible at 1.0 Tesla with respect to the Solomon contribution.

The hyperfine shift

The analysis of the NMR spectra of a paramagnetic system passes through the evaluation of the hyperfine shifts, which correspond to the differences in the NMR shifts collected for the paramagnetic system and its diamagnetic analogue.

In solution, both the Fermi-contact and the dipolar contributions are averaged by molecular tumbling, which causes sampling of all molecular orientations with respect to the applied magnetic field. The rotational average of the dipolar shift is called PCS and is commonly analysed in terms of its dependence on a symmetric, traceless tensor ($\boldsymbol{\Delta\chi}$), corresponding to the anisotropic part of the magnetic susceptibility tensor, $\boldsymbol{\chi}$.[23]

In the point-dipole approximation, the equations for PCSs and FCSs in isotropic solutions are:

$$\delta^{pc} = \frac{1}{12\pi r^3}\mathrm{Tr}\left[\boldsymbol{\chi} \cdot \left(\frac{3\mathbf{r}\mathbf{r}^T}{r^2} - \mathbf{1}\right)\right] \quad (5)$$

$$\delta^{Fc} = \frac{A^{FC}}{3\mu_0\hbar\gamma_I\mu_B}\mathrm{Tr}\left[\boldsymbol{\chi} \cdot \left[\mathbf{g}^T\right]^{-1}\right] \quad (6)$$

where **r** is the distance vector of the nucleus I from the paramagnetic metal nucleus, and the Fermi contact coupling constant is defined as:

$$A^{Fc} = \frac{\mu_0}{3}\hbar\gamma_I\mu_B g_e \frac{\rho_I}{S} \quad (7)$$

and other symbols have the usual meaning. These equations for the pseudocontact and Fermi-contact shifts (written without using tensor notation) were derived for the first time by Kurland and McGarvey[23] in 1970.

Because the term $(3\mathbf{r}\mathbf{r}^T/r^2 - 1)$ appearing in eqn (5) is traceless, δ^{pc} is only determined by the susceptibility anisotropy $\boldsymbol{\Delta\chi} = \boldsymbol{\chi} - \chi_{iso}\mathbf{1}$, where $\chi_{iso} = \mathrm{Tr}(\boldsymbol{\chi})/3$, whereas δ^{Fc} depends on the overall $\boldsymbol{\chi}$ tensor. In the reference frame where the $\boldsymbol{\Delta\chi}$ tensor is diagonal, eqn (5) becomes

$$\delta^{pc} = \frac{1}{12\pi r^3}\left[\Delta\chi_{ax}(3\cos^2\theta - 1) + \frac{3}{2}\Delta\chi_{rh}\sin^2\theta\cos 2\varphi\right] \quad (8)$$

where

$$\Delta\chi_{ax} = \chi_{zz} - \frac{\chi_{xx} + \chi_{yy}}{2} = \frac{3}{2}(\chi_{zz} - \chi_{iso}), \qquad \Delta\chi_{rh} = \chi_{xx} - \chi_{yy} \quad (9)$$

and r, θ and φ are the spherical coordinates of the nucleus in the principal frame of the $\boldsymbol{\chi}$ tensor, with the origin in the position of the unpaired electron(s), and χ_{xx}, χ_{yy} and χ_{zz} corresponding to the eigenvalues of the $\boldsymbol{\chi}$ tensor (the z and x directions being defined so that $|\Delta\chi_{rh}| \leq 2\ |\Delta\chi_{ax}|/3$ and $|\chi_{xx} - \chi_{yy}| < |\chi_{xx} - \chi_{zz}|$). PCSs thus contain valuable structural information, and hence they have been shown useful as restraints for protein structure determination.[24–31]

Using a modern quantum chemistry (QC) formalism, in the spin Hamiltonian approximation, at high temperature ($\mu_B B_0 \ll kT$) and for a system with a singly-populated non-degenerate ground multiplet, the paramagnetic susceptibility tensor can be written in the form

$$\boldsymbol{\chi} = \frac{\mu_0\mu_B^2}{kT}\mathbf{g} \cdot \langle \mathbf{S}\mathbf{S}^T \rangle \cdot \mathbf{g}^T \quad (10)$$

where $\langle \mathbf{SS}^T \rangle$ is the effective electron spin dyadic equal to

$$\langle S_\alpha S_\beta \rangle = \frac{\sum_{ij} Q_{ji} \langle \psi_i | S_\alpha | \psi_j \rangle \langle \psi_j | S_\beta | \psi_i \rangle}{\sum_i \exp\left[-\tilde{E}_i^{(0)}/(kT)\right]}, \quad \alpha, \beta = \{x, y, z\} \quad (11)$$

$$Q_{ji} = \begin{cases} \exp\left[-\tilde{E}_i^{(0)}/(kT)\right] & \text{for } \tilde{E}_i^{(0)} = \tilde{E}_j^{(0)} \\ -\dfrac{kT}{\tilde{E}_j^{(0)} - \tilde{E}_i^{(0)}} \left\{ \exp\left[-\tilde{E}_j^{(0)}/(kT)\right] - \exp\left[-\tilde{E}_i^{(0)}/(kT)\right] \right\} & \text{for } \tilde{E}_i^{(0)} \neq \tilde{E}_j^{(0)} \end{cases}$$

and $\tilde{E}_i^{(0)}$ is the energy of the state $|\psi_i\rangle$ at zero magnetic field. In the approximation to the first order in $D/(kT)$, this provides[32]

$$\langle \mathbf{SS}^T \rangle = \frac{S(S+1)}{3}\mathbf{1} - \frac{S(S+1)(2S-1)(2S+3)}{30kT}\mathbf{D} \quad (12)$$

where $\mathbf{D}$ is the ZFS tensor.

A question recently was raised on the correctness of eqn (5) and (10), *i.e.* in the derivation of the relationship between the tensor used to describe the PCSs, and the $\mathbf{g}$ and $\mathbf{D}$ tensors.[33–41] PCSs can in fact be calculated using QC approaches as a part of total hyperfine shifts.[34,39,40,42–48] Using the effective spin Hamiltonian framework, it was first clarified that if the contribution of the orbital angular momenta of electrons to the PCSs is not correctly included in the first-principles QC treatment, a different expression for the PCSs is obtained.[49] The validity of eqn (5) and (10) was finally demonstrated[50,51] using the QC formulation of hyperfine shifts to be proportional to the second derivative of the thermally averaged Helmholtz free energy F with respect to the magnetic field and the nuclear magnetic moment, calculated at zero magnetic field and zero magnetic moment.[52] In the effective spin Hamiltonian framework, the PCSs can in fact be written as

$$\delta^{\text{pc}} = -\frac{1}{3}\text{Tr}\left[-\frac{\mu_\text{B}}{\hbar\gamma_I kT}\mathbf{g} \cdot \langle \mathbf{SS}^T \rangle \cdot \mathbf{A}^T\right] \quad (13)$$

where the hyperfine coupling tensor $\mathbf{A}$ is composed of the spin dipolar, paramagnetic spin–orbit and gauge contributions. The gauge contribution is necessary to preserve gauge invariance in the presence of spin–orbit coupling.[50,51] At the level of second-order degenerate perturbation theory, in the long-range limit, eventually it was shown that

$$\mathbf{A} = \mathbf{A}^{\text{SD}} + \mathbf{A}^{\text{PSO/SOC}} + \mathbf{A}^{\text{gauge}} = \frac{\mu_0}{4\pi}\frac{\hbar\gamma_I\mu_\text{B}}{r^3}\left(\frac{3\mathbf{rr}^T}{r^2} - \mathbf{1}\right) \cdot \mathbf{g} \quad (14)$$

in agreement with eqn (5) and (10), because $\mathbf{A}^{\text{SD}} = \frac{\mu_0}{4\pi}\frac{\hbar\gamma_I\mu_\text{B}}{r^3}\left(\frac{3\mathbf{rr}^T}{r^2} - \mathbf{1}\right)g_\text{e}$ and $\mathbf{A}^{\text{PSO/SOC}} + \mathbf{A}^{\text{gauge}} = \frac{\mu_0}{4\pi}\frac{\hbar\gamma_I\mu_\text{B}}{r^3}\left(\frac{3\mathbf{rr}^T}{r^2} - \mathbf{1}\right) \cdot (\mathbf{g} - g_\text{e}\mathbf{1})$. This derivation confirms the validity of the classical equations for PCSs and thus paves the way for their predictions from the $\boldsymbol{\chi}$ tensors which can possibly be calculated through QC tools.

The relationships between PCSs, the $\boldsymbol{\Delta\chi}$ tensor and the $\mathbf{g}$ tensor were also experimentally demonstrated to be correctly described by eqn (5) and (10) for some copper(II) proteins, where the $\mathbf{g}$ tensor could be measured through EPR under the same conditions of the NMR experiments.[53]

Eqn (5) for PCSs is valid in the point-dipole approximation, which assumes that the unpaired electron(s) are localized onto the paramagnetic atom. If, on the contrary, the unpaired electron spin(s) are spread over the ligand atoms through molecular orbital overlap, PCS values should be calculated from integration performed over space by considering the actual electron density distribution.[25] In the assumption that the $\boldsymbol{\chi}$ tensor is independent of the electron spin positions, a relationship – called the Inverse Kuprov Equation – was recently found that permits to recover the electron density distribution, under some regularization conditions, from the experimental PCSs and the atomic coordinates of the molecule.[25,54]

The paramagnetic residual dipolar couplings

The anisotropy of the magnetic susceptibility causes partial self-orientation of paramagnetic molecules. In fact, the probabilities for different molecular orientations with respect to the magnetic field are not equal and depend on the anisotropy of the $\boldsymbol{\chi}$ tensor. The principal components of the self-alignment tensor are given by $p_{\text{ii}} = \frac{1}{3}\left[1 + \frac{B_0^2}{5\mu_0 kT}(\chi_{\text{ii}} - \chi_{\text{iso}})\right]$.[12,55] This partial self-alignment of the molecules causes a non-null average of the energy of the dipole–dipole interaction between the nuclear magnetic moments, and thus this results in a paramagnetic contribution to their ^1J coupling. Therefore, pRDCs are usually calculated from the differences of the J-couplings measured for paramagnetic and diamagnetic samples (assuming negligible dynamic frequency shifts[12]). As a result, pRDCs and PCSs depend on the same magnetic susceptibility anisotropy tensor $\boldsymbol{\Delta\chi}$ of the paramagnetic metal ion, and are thus often analyzed jointly. Nevertheless, as the dependences on the structural parameters are different, PCSs and pRDCs bear complementary information. In the reference frame where the $\boldsymbol{\Delta\chi}$ tensor is diagonal, pRDCs are equal to

$$\Delta\nu^{\text{prdc}} = -\frac{S_{\text{LS}}}{4\pi}\frac{B_0^2}{15kT}\frac{\hbar\gamma_{\text{I1}}\gamma_{\text{I2}}}{2\pi {r_{12}}^3} \times \left[\Delta\chi_{\text{ax}}\left(3\cos^2\alpha - 1\right) + \frac{3}{2}\Delta\chi_{\text{rh}}\sin^2\alpha\cos 2\beta\right] \quad (15)$$

where α and β are the spherical angles describing the orientation of the internuclear $\mathbf{r}_{12}$ vector in the main frame of the $\boldsymbol{\chi}$ tensor. Note that pRDCs depend on the nuclear magnetogyric ratio (PCSs do not depend on the observed nuclei) and on the square of the applied magnetic field (PCSs are field independent, until approaching saturation conditions), whereas they are independent of the nuclear distance from the paramagnetic metal ion (PCSs depend on r^{-3}). The term S_{LS} is a Lipari-Szabo order parameter[56] which amounts to 1 for completely rigid systems, but is smaller than 1 in the presence of some local mobility.

In the presence of paramagnetic tags attached to proteins with some degrees of flexibility, the pRDCs are significantly

smaller than the values that are calculated for rigid systems using the $\Delta\chi$ tensor. In turn, when pRDCs are analysed using eqn (15) with $S_{LS} = 1$, as routinely done, "effective $\Delta\chi$ tensors" are obtained that may be significantly smaller than the real $\Delta\chi$ tensors. The different sizes of PCS-derived and pRDC-derived $\Delta\chi$ tensors can be in fact used to pinpoint the occurrence of tag mobility.

Relation between PCSs and RDCs

PCSs and pRDCs can be fitted against the same molecular structural models to obtain the magnetic susceptibility anisotropy tensors, $\Delta\chi$, on which they depend (see eqn (5) and (15)), using programs like FANTEN[57] or NUMBAT.[58] Because PCSs and pRDCs depend on the same tensor, they can fit simultaneously, provided that the biomolecular structure is rigid, and a slight possible reduction in the orienting tensor ($S_{LS} < 1$) is allowed for, taking into account some local mobility of the coupled nuclei vectors.

Magnetic susceptibility anisotropy and electron relaxation rates of paramagnetic metals

As seen in the previous sections, the magnitudes of PCSs and pRDCs increase with the anisotropy of magnetic susceptibility, whereas PREs are the functions of the electron relaxation time and of the overall magnetic susceptibility (besides of the molecular reorientation time). Magnetic susceptibility anisotropies and electron relaxation times in turn depend on the presence of excited states close in energy (with respect to kT) to the ground state, which makes spin–orbit coupling efficient. Metal ions with low-lying excited states thus have (i) very efficient electron relaxation mechanisms, so that their electron relaxation times are very short, and (ii) very anisotropic $\mathbf{g}$ tensors, so that their magnetic susceptibility anisotropies are very large. Therefore, these systems originate from small Solomon contributions to PREs and large PCSs and pRDCs. Conversely, systems with excited states far in energy from the ground state have long electron relaxation times and small magnetic susceptibility anisotropies, so that Solomon contributions to PREs are large and PCSs and pRDCs are small. Fig. 1 and 2 show the typical values of τ_e, χ and $\Delta\chi$ for the first row transition metal ions and lanthanoids. The figures also show the maximum distances from the nuclei of the paramagnetic metal (those in axial position) experiencing a PCS as small as 0.05 ppm. These distances are calculated from the expression $r = \left(\frac{\Delta\chi_{ax}}{6\pi \times 0.05 \times 10^{-6}}\right)^{1/3}$.

Large PREs determine the presence of a blind sphere around the paramagnetic metal, where nuclear signals are undetectable in standard NMR experiments due to the excessive paramagnetic line broadening. Curie relaxation can sizably contribute to the PREs in large molecules (due to the large τ_r), as in metalloproteins, especially in the case of late lanthanoids, when χ is quite large. Fig. 3 and 4 show typical R_2 ^{1}H PREs for a proton at 10 Å from the metal, in a molecule with the τ_r of 10 ns,

	Ti(II)	V(IV)	Cr(III)	Mn(II)	Mn(III) HS	Fe(III) HS	Fe(III) LS	Fe(II) HS	Co(II) HS	Co(II) LS	Ni(II)	Cu(II)
S	1/2	1/2	3/2	5/2	2	5/2	1/2	2	3/2	1/2	1	1/2
g_e	2	2	2	2	2	2	2	2	2	2	2	2
τ_e (high field)	30 ps	1-20 ns	0.2 ns	100 ns	50 ps	0.01-1 ns	1 ps	1 ps	1-10 ps	100 ps	1-100 ps	1-3 ns
χ (10^{-32} m^3)	2.6	2.6	13	31	21	31	2.6	21 (23-27)	13 (15-24)	2.6 (2.8-5.5)	7 (7-14)	2.6 (2.6-4.2)
$\Delta\chi_{ax}$ (10^{-32} m^3)	0.4	0.1	< 0.1	< 0.1	0.5	3.0	2.4	2.1	3.0-7.0	1.0	0.2-2.0	0.6

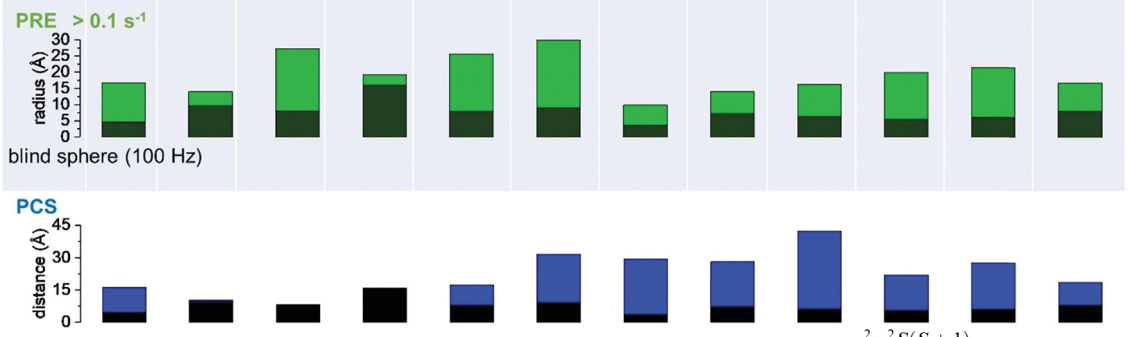

Fig. 1 Typical values of electron relaxation time (τ_e), magnetic susceptibility (χ, spin-only values, equal to $\frac{\mu_0\mu_B^2 g_e^2 S(S+1)}{3kT}$, and effective values, reported in parenthesis) and its axial anisotropy ($\Delta\chi_{ax}$) of transition metal ions. The typical radii of blind spheres (black) and spheres with ^{1}H PREs larger than 0.1 s^{-1} (green), and the maximum distances of nuclei in axial position with PCSs of 0.05 ppm (blue) are also shown for a protein with the reorientation time of 10 ns at 700 MHz (HS = high spin, LS = low spin).

	Ce(III)	Pr(III)	Nd(III)	Sm(III)	Eu(III)	Gd(III)	Tb(III)	Dy(III)	Ho(III)	Er(III)	Tm(III)	Yb(III)
J	5/2	4	9/2	5/2	-	7/2	6	15/2	8	15/2	6	7/2
g_J	6/7	4/5	8/11	2/7	-	2	3/2	4/3	5/4	6/5	7/6	8/7
τ_e	0.20 ps	0.25 ps	0.46 ps	0.16 ps	0.01 ps	~100 ns	0.69 ps	0.98 ps	0.81 ps	0.78 ps	1.5 ps	0.48 ps
χ (10^{-32} m^3)	5.6	11	11	0.6	~6	55	83	99	99	80	50	18
$\Delta\chi_{ax}$ (10^{-32} m^3)	2.1	3.4	1.8	0.2	-2.4		42.0	34.8	18.9	12.2	25.9	8.4
$\Delta\chi_{rh}$ (10^{-32} m^3)	-0.8	-2.0	-0.4	-0.07	-1.5		-11.5	-20.0	-5.2	-7.5	-12.0	-5.3

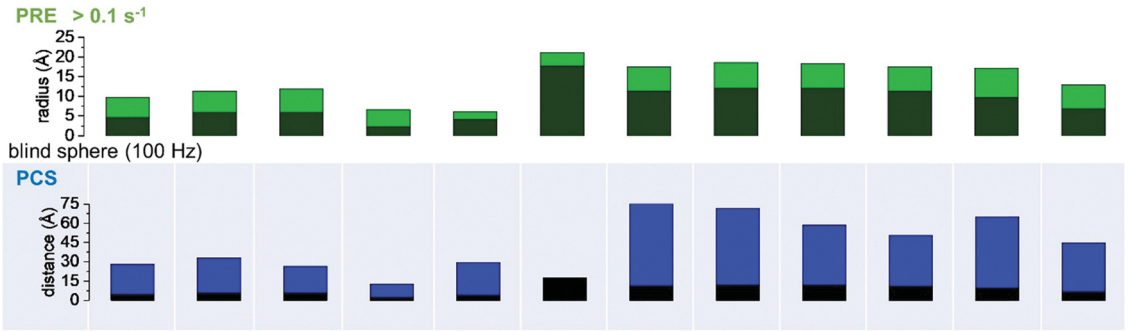

Fig. 2 Typical values of electron relaxation time (τ_e), magnetic susceptibility (χ) and axial and rhombic anisotropy ($\Delta\chi_{ax}$ and $\Delta\chi_{rh}$) of lanthanoid ions. The typical radii of blind spheres (black) and spheres with ^{1}H PREs larger than 0.1 s^{-1} (green), and the maximum distances of nuclei in axial position with PCSs of 0.05 ppm (blue) are also shown for a protein with the reorientation time of 10 ns at 700 MHz.

at 900 MHz, and the radius of the ^{1}H blind spheres for the different metal ions. Blind sphere radii are also shown in Fig. 1 and 2 together with the radii of the spheres containing nuclei with R_1 ^{1}H PREs larger than 0.1 s^{-1} (taken as detection limit).

Lanthanoid binding tags rigidly attached to diamagnetic systems[59–62] or specific lanthanoid-binding sites introduced in diamagnetic proteins[63] are conveniently used for the generation of paramagnetic data to be used as structural restraints in the study of diamagnetic biomolecules. It was recently made clear that the choice of the lanthanoid ligand can significantly affect the magnitude of the magnetic susceptibility anisotropy, and thus of the PCSs, even in the assumption of a completely rigid attachment to the biomolecule. The need for a rigid attachment of the paramagnetic site is mandatory for avoiding conformational averaging effects at the origin of a reduction in the "effective" $\boldsymbol{\Delta\chi}$ tensor (see above – although an average tensor may even not be defined when the position of the metal with respect to the molecule changes), and thus on the measured PCSs and pRDCs.[64]

The dependence of the $\boldsymbol{\Delta\chi}$ tensor on the coordination environment of lanthanoid ions, usually neglected due to the assumption that the ligand field splitting is small compared to the large spin–orbit coupling of lanthanoids, originates from the observation that in lanthanoid complexes, ligand field splittings are commonly larger than kT at room temperature,[65] and the electron density distribution is not spherical in f orbitals, except that for gadolinium(III). The $\boldsymbol{\Delta\chi}$ tensor has been shown to depend on the compliance of the single-ion electron density with the crystal field environment in which it is placed. The $(2J+1)$-fold degeneracy of the ground state can in fact be removed by the surrounding crystal field, so that the electronic structure of the ground state is linked to the strength and symmetry of the ligand field.[66,67] In turn, a proper choice of the coordination environment of the lanthanoid ion can increase the performance of lanthanoid tags.

As described in ref. 66 and 67, there are two general optimum ligand architectures providing a highly anisotropic ground state depending on whether the basic overall shape of the free-ion electron density is oblate, as for Ce^{3+}, Pr^{3+}, Nd^{3+}, Tb^{3+}, Dy^{3+} and Ho^{3+}, or prolate, as for Pm^{3+}, Sm^{3+}, Er^{3+}, Tm^{3+} and Yb^{3+}. The magnetic susceptibility anisotropy of an oblate ion is maximized by a crystal field for which the ligand electron density is concentrated above and below the xy plane (see Fig. 5), so that the ground state corresponds to the configurations that minimize repulsive charge contacts between ligand and f-electron charge clouds. This configuration corresponds to the m_J state with the highest value. At the same time, states with low m_J values force the f-electron charge cloud into direct contact with the ligands, thus having a high energy. Conversely, the magnetic susceptibility anisotropy of a prolate ion is maximized by an equatorial coordination geometry so that the ground state, minimizing the charge contact with the axially located f-element electron density, corresponds to the m_J state with the highest value. Also the main direction (z axis) of the $\boldsymbol{\Delta\chi}$ tensor depends on the non-spherical electron density distribution of the lanthanoid ion and on the ligand atom positions,[68,69] so as it may be oriented differently for the different lanthanoids, even if they are bound by the same

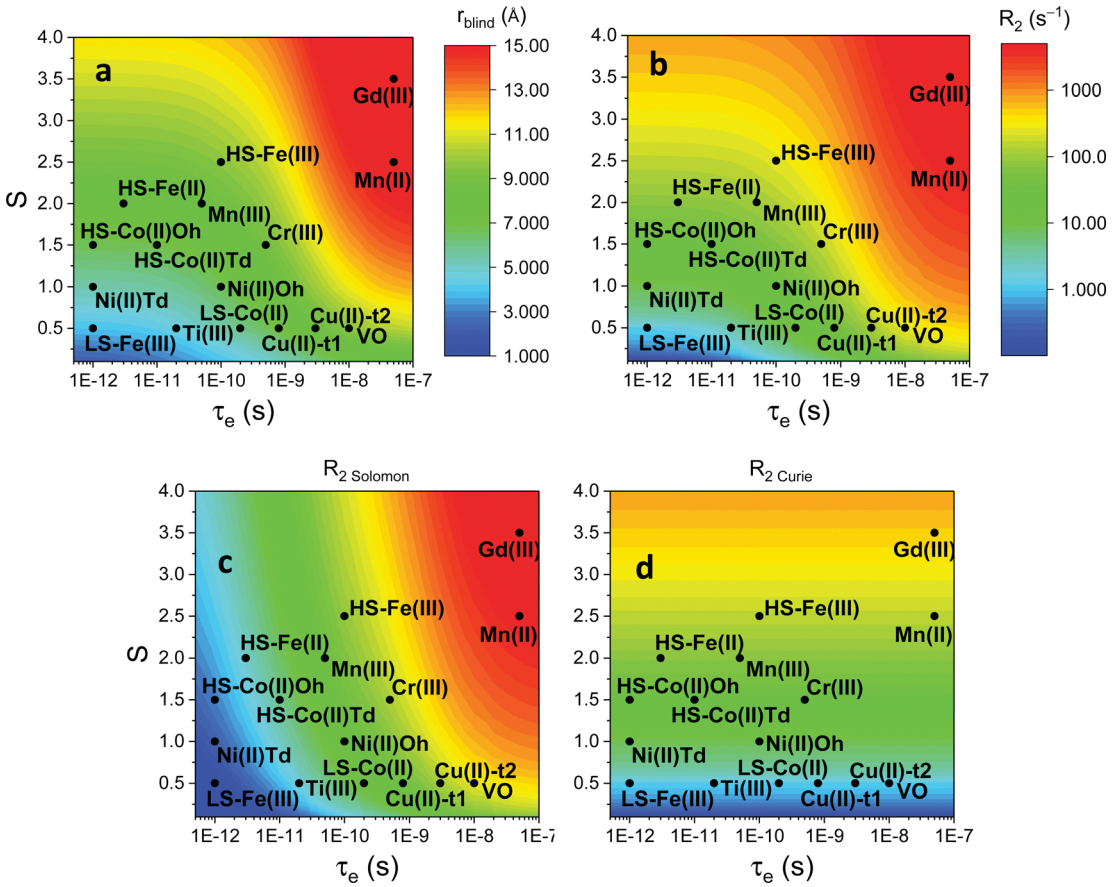

Fig. 3 (a) Typical radii of ^{1}H blind spheres at 900 MHz (paramagnetic linewidths ≥100 Hz), for molecules with the τ_r of 10 ns and typical values of the electron relaxation times of paramagnetic metal ions. (b) ^{1}H R_2 PREs and their Solomon (c) and Curie (d) contributions at 900 MHz, for a proton at 10 Å from the metal, in a molecule with the τ_r of 10 ns. Besides transition metal ions, only gadolinium(III) is shown in this figure; other lanthanoids, differing in their g-values, are reported in Fig. 4. Metals are labeled as LS: low spin; HS: high spin; t1: type-1; t2: type-2; Td: tetrahedral coordination; Oh: octahedral coordination.

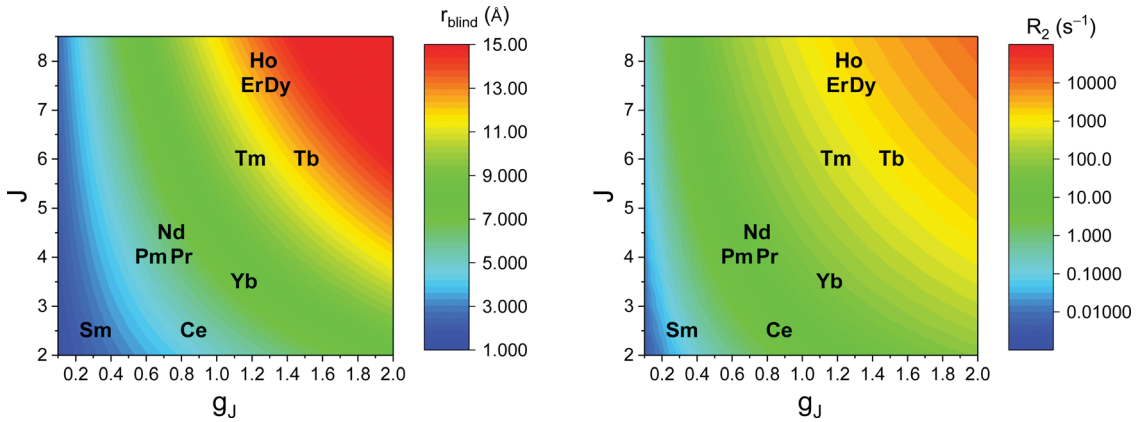

Fig. 4 Typical radii of ^{1}H blind spheres of lanthanoid(III) ions (paramagnetic linewidths ≥100 Hz, left panel), and ^{1}H R_2 PRE (right panel), due to Curie relaxation, for a proton at 10 Å from the lanthanoid ion, at 900 MHz. The electron relaxation times τ_e are set to 1 ps and τ_r to 10 ns. Gadolinium(III), with τ_e several orders of magnitude larger, is shown in Fig. 3.

ligand and, likewise, it may be oriented differently for different ligands, even if bound to the same lanthanoid ion. Careful engineering can lead to ligands preserving an almost completely axial susceptibility even at room temperature in solution. For example, a dysprosium(III) complex is available with $\Delta\chi_{ax}$ = 2.16 × 10^{-30} m^3, which is more than 220% of its isotropic magnetic susceptibility, and $\Delta\chi_{rh}$ = 2.17 × 10^{-32} m^3, which is less than 3% of its isotropic value.[70]

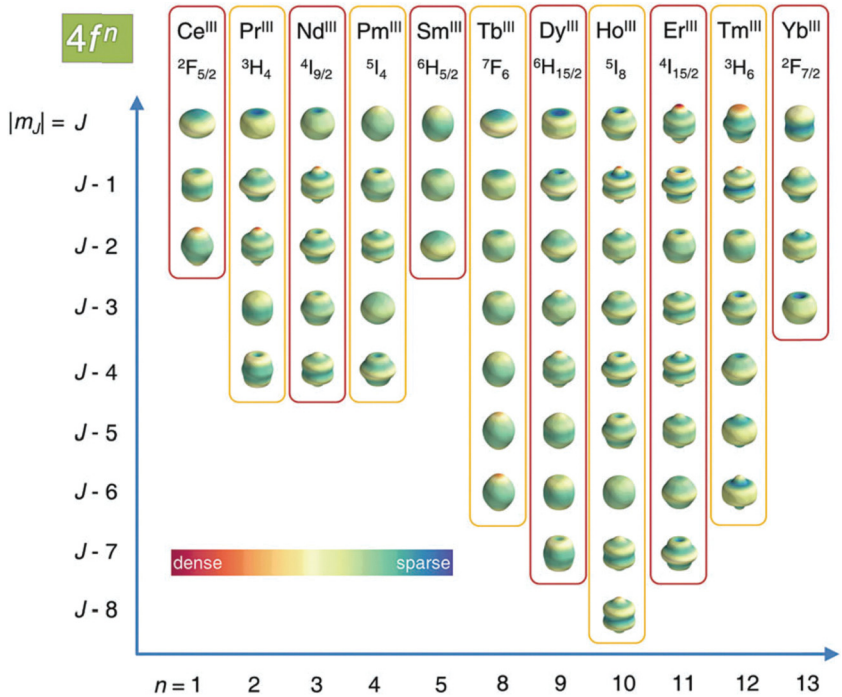

Fig. 5 Charge density angular distribution for lanthanoid(III) 4f shells for the different m_J states. Reproduced from ref. 66 with permission from the Royal Society of Chemistry.

The magnetic susceptibility anisotropy values obtained for lanthanoids in calbindin D_{9k}, reported in Fig. 2, can be compared to the values obtained for some DOTA-based complexes, for tris(dipicolinato)lanthanoids (dipic = pyridine-2,6-dicarboxylate), and for some widely used and efficient lanthanoid-binding tags, shown in Fig. 6. The anisotropy values were determined from the shifts of the ligand nuclei in the case of the DOTA,[71] DOTA-M8,[72] DOTA-M7FPy[72] and tris(dipicolinato)[73,74] complexes, and from

	Tb	Dy	Tm	Yb
Calbindin D_{9k}	42, -11	35, -20	26, -12	8.4, -5.3
DOTA-M8		-80, 0	104, 0	
DOTA-M7FPy	62, -31	101, -24	83, -8	23, -8
DOTA	-50, 0	-59, 0	63, 0	19, 0
Tris(dipicolinato)	-29, 0	-30, 0	20, 0	6, 0
CLaNP-5	-45, 16	-36, 15	55, -6.9	9, -2.3
BrPSPy-DO3M(S)A		46, -13	45, -12	10, -6
Ln-M7-Nitro	64, -22	96, -13	71, -6.2	14, -7.5

Fig. 6 Magnetic susceptibility anisotropy tensors ($\Delta\chi_{ax}$, $\Delta\chi_{rh}$, in 10^{-32} m^3) and isosurfaces of PCS = 0.05 ppm (in blue) or −0.05 ppm (in red) for some lanthanoid ions in different coordination geometries. Axis values are in Å.

the nuclear shifts of the attached proteins in the case of the tags CLaNP-5,[28,75] BrPSPy-DO3M(S)A[76] and Ln-M7-Nitro.[77] In the case of the proteins with paramagnetic tags, the shifts may be reduced to some extent by a non-completely rigid attachment of the tag.

The data show that if the DOTA-based tags providing the largest anisotropies could be rigidly attached to proteins, PCSs could be detected for nuclei at larger distances than expected from the $\Delta\chi$ of the same ions in calbindin D_{9k}, and higher, and thus more accurate, pRDCs could be measured, thus extending the perspectives for their use in the structural determination of biomolecular systems.

Paramagnetic structural restraints

Paramagnetic restraints efficiently provide structural information throughout the whole macromolecular system, or a large part of it because of their long-range nature. This feature becomes particularly relevant when paramagnetic restraints are used in integration with the data obtained using other techniques, and can help in removing assignment ambiguities.[11,78–82] Besides the use for *de novo* structural determination, the interest towards paramagnetic restraints has increased in the last decades,[83] thanks to other notable implications of their use in (*e.g.*) detecting transient interactions, conformational changes, *etc.*

Paramagnetic restraints in the protein structure calculation

Determination of the traditional structure by NMR suffers from the lack of long-range observables. The collected PCSs, pRDCs and PREs can thus be used for the calculation of *de novo* structure or for the refinement of structures together with dihedral angle restraints and other diamagnetic restraints in programs like PARAMAGNETIC-CYANA[84,85] or Xplor-NIH.[86,87] For instance, the solution structure of the protein calbindin D_{9k} could be refined using paramagnetic data from lanthanoid ions substituted in the second calcium binding site of the protein, with an increase in resolution not only in the close proximity of the paramagnetic center but along the overall protein backbone chain.[88] A further insight into the structure of calbindin D_{9k} with the thulium(III) ion substituting one calcium(II) ion arose from the application of the Inverse Kuprov Equation: a probability density distribution of the paramagnetic center was reconstructed, providing a better agreement with the experimental data than calculated from the point-dipole approximation.[25]

PCSs can efficiently guide the reconstruction of protein conformations in the ROSETTA fragment assembly method,[24] especially when multiple paramagnetic metals positioned in different places on the protein surface are used.[89,90] Also PREs showed usefulness to recover protein structures in molecular fragment searching protocols, when used in conjunction with diamagnetic RDCs and/or backbone dihedral angles.[91,92] In microcrystalline protein samples, PCSs have been used to obtain unambiguous signal assignments in solid-state NMR spectra, allowing for determining high-resolution protein structure,[93,94] as well as for determining the relative positions of the protein molecules in the crystal.[31]

Interdomain position reorganization in solution and crystals

Also the solution structure of calmodulin in complex with the calmodulin-binding peptide of the death-associated protein kinase could be determined using PCSs and pRDCs from three different lanthanoids substituted into the second binding site of the N-terminal domain of the N60D mutant of the protein.[95] The calculated structure shows a different arrangement of the two domains with respect to the crystal structure: this is due to the absence of inter-protein contacts that are present in the crystal. Indeed, this solution structure resulted in better agreement with the crystal structure of calmodulin in complex with the whole kinase protein[96] than with the crystal structure of calmodulin bound to the peptide (Fig. 7a).[97] The steric hindrance of the whole protein in the crystal prevents the formation of H-bonds and salt bridges between different calmodulin molecules, thus allowing the latter to have a conformation more similar to the solution structure. The residual discrepancy between the paramagnetic data and the solution structure can be attributed to a limited but significant interdomain mobility.[98] In general, the achievement of a good fit of the

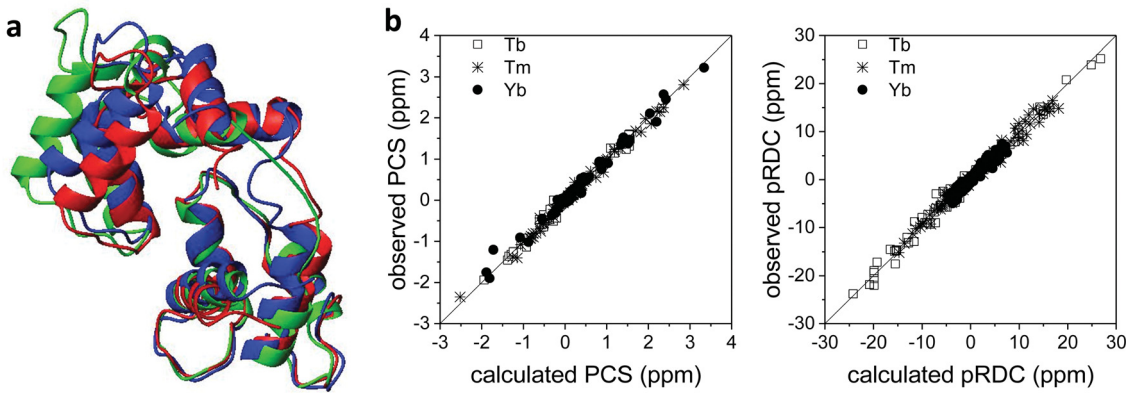

Fig. 7 (a) X-ray structure (PDB entry 1YR5, in red) and refined solution structure (PDB entry 2K61, in blue) of the peptide-bound calmodulin, and X-ray structure of calmodulin in complex with the whole kinase protein (PDB entry 2X0G, in green). (b) Best fit of PCSs and pRDCs for the refined solution structure, calculated using FANTEN[57] and a common $\Delta\chi$ tensor for each paramagnetic metal ion.

experimental PCSs and pRDCs[30,57,97] is an indication of a good accuracy of the protein structure (Fig. 7b).

Paramagnetic data for protein structural refinement in integrative structural biology

The long-range nature of paramagnetic restraints is particularly appealing to validate, and possibly refine, structures obtained from X-ray data, cryo-electron microscopy, or homology modeling. X-ray crystallography, in particular, provides very precise protein structures, which can, however, suffer from crystal packing forces. Therefore, they can be inaccurate models, to some extent, in solution, where these interactions are abolished. Furthermore, crystal structures are affected by "structural noise",[99] depending on the resolution of the X-ray reflections and on the structural refinement protocol employed, which may result in a lower accuracy of local structural details than that contained in NMR data. The high accuracy, despite their sparsity, of paramagnetic restraints makes them fully complementary to X-ray data for achieving a more accurate structural description of the biomolecules, also because NMR data provide direct information on local details, in the form of interatomic distances or orientations of vectors connecting chemically bound nuclei.[30]

The information contained in PCSs and pRDCs are of different kinds. On the one hand, PCSs are barely affected by small structural inaccuracies, so that they are nicely fitted when the structural model is in overall agreement with the biomolecular structure in solution. Their fit provides a very robust estimation of the magnetic susceptibility anisotropy tensor, being determined by several tens, or hundreds, of PCS values. On the other hand, pRDCs, which are sensitive to even small local inaccuracies in the orientation of nuclear pairs, hardly agree with the susceptibility tensor obtained from PCSs unless the molecular structure is a very accurate model for the protein in solution. For instance, the pRDCs measured for the catalytic domain of matrix metalloproteinase-1 (MMP1), attached with the CLaNP-5 tag[62] with either one of the three paramagnetic lanthanoids Tb^{3+}, Tm^{3+} and Yb^{3+}, provide an agreement with the crystallographic structure much poorer than that expected from the experimental errors of the data (Fig. 8), despite the very good fit of the PCS data.[29] This disagreement could be due to either some protein structural rearrangements on passing from the crystal state to the solution state, or to some inaccuracy in the nuclear coordinates determined from X-ray data (structural noise). Actually, the second case seems more plausible for this system because the disagreement of pRDCs could be solved by very small conformational adjustments, within the indeterminated X-ray data. Similarly, the disagreement between the diamagnetic RDCs measured for the protein ubiquitin and its crystal structure could be accommodated within the structural noise of the X-ray data,[29] and even for sub-atomic resolution structures of lysozyme[100] RDC restraints could be accommodated within the X-ray structural noise without the need for invoking conformational averaging.

The paramagnetic data can thus be used to assess how accurately crystal structures represent solution structures and to improve them by simultaneous refinements through NMR and X-ray data. PCSs and pRDCs can be fitted, using the same $\Delta\chi$ tensor for each metal ion, together with X-ray data using the program REFMAC-NMR[29] developed within REFMAC5 from CCP4.[101] The program provides a refined structure, resulting from the combined use of the information on the heavy atom positions mainly contained in X-ray reflections, and on nuclear (mostly hydrogen) positions and bond orientations of nuclear pairs contained in PCSs and pRDCs. If this structure is in good agreement with both X-ray data (in terms of *R* and *R*-free values) and NMR data (in terms of Q-factor), it can be concluded that there are no inconsistencies between the crystal and the solution structures, and thus the refinement performed with both NMR and X-ray data provides a more reliable structural model.[102] On the other hand, the presence of some NMR data which do not match the values predicted by the refined conformation within their error is an indication of minor inconsistencies, *i.e.*, of local conformational rearrangements between the solution and the solid states (or the presence of conformational heterogeneity in solution) in specific regions of the protein.[30,102]

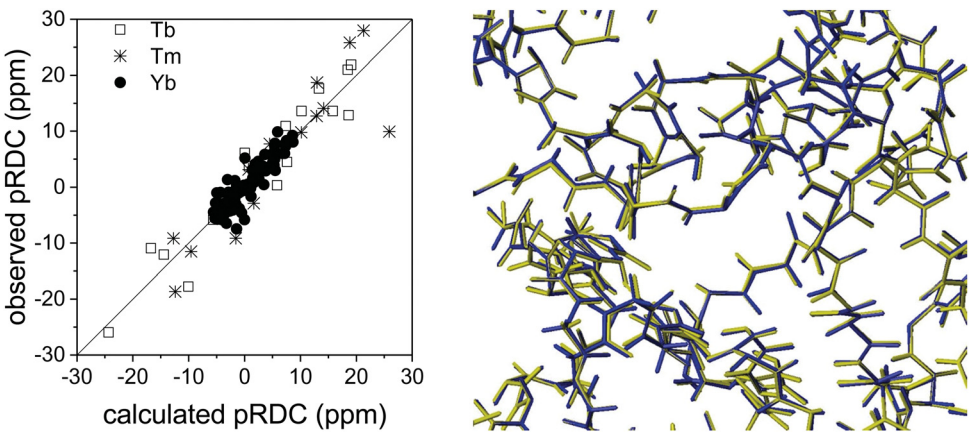

Fig. 8 Best fit agreement of experimental pRDCs measured for the catalytic domain of matrix metalloproteinase-1 with the crystallographic structure (PDB entry 3SHI) (2.2 Å resolution) and superposition of original (in blue) and refined (in yellow) structures.

In the case of the catalytic domain of MMP1, REFMAC-NMR provides a refined structure with a backbone root mean square deviation from the original model of only 0.04 Å (Fig. 8), in full agreement with the X-ray reflections and a significant overall improvement in the agreement of the NMR data, the Q-factor of the pRDCs decreasing from 0.41 to 0.16.[29] This example shows the high accuracy in defining structural details that these NMR data can provide.

For systems composed of multiple domains, the evaluation of the $\Delta\chi$ tensors determined from the fit of PCSs and/or pRDCs measured for each domain provides a simple but powerful way for assessing their relative arrangement in solution. Several situations can be encountered.

1. If both sizes and orientations of the tensors coincide, the crystal conformation is maintained in solution.

2. If only the sizes coincide, and not the orientations, the relative arrangements of the refined domains in solution can be retrieved by superimposing the anisotropy tensors.[57] As an example, a cobalt(II) binding tag was attached to the N-terminal domain of the homodimeric protein STAT4. The PCSs permitted to refine the monomeric structure[80] and to determine the arrangement of the monomeric subunits. Sub-stoichiometric addition of the paramagnetic metal in this case permitted to disrupt the symmetry in the NMR spectra of the protein.[103] Data from multiple paramagnetic ions or from ions located in multiple positions are often needed to identify the correct conformation among the possible degenerate solutions.[104,105]

3. Finally, if the tensors differ both in size and in orientation, interdomain mobility occurs and thus conformational averaging takes place.[64] In these conditions, the measured PCSs, pRDCs and PREs are population-weighted averaged over all sampled conformations (PREs may also depend on the time of interconversion between the different conformations).[106,107] Several approaches have been developed to recover some information on the experienced conformations, although the reconstruction of the real structural ensemble is impossible due to the inherent presence of degenerate solutions.[64,108–113]

PREs, providing very sensitive information on the distance between the observed nucleus and the paramagnetic metal ion (eqn (1) and (2)), have been found to be very useful to monitor the occurrence of structural mobility in solution. In particular, PREs can detect the presence of less (few percent) populated conformational states when the latter imply metal–nuclear distances much shorter than in the more populated conformational states.[114] In the presence of two states, in fact, if their exchange rate is faster than the difference in relaxation rates and slower than the reorientation time of the system, the measured PREs are population weighted averages of the PREs in the two states. Along the same lines, PREs have been used to detect the presence of transient, sparsely populated, protein–protein encounter complexes, and to identify the patches of protein residues that come into short-lived close contact with one another.[115–117] Such sensitivity of PREs to lowly populated structural states is an extraordinary informative tool for the characterization of transient states in solution. Paramagnetic restraints can also be used in HADDOCK[118] for driving docking calculations of protein complexes.

Coupling QC calculations to paramagnetic data analysis

Quantum chemical methods for the calculation of hyperfine shifts and relaxation rates are becoming increasingly accessible and can now be included in the toolkit for protein structural calculations. The hyperfine shifts of the two high-spin pentacoordinate nickel(II) complexes, NiSAL-MeDPT and NiSAL-HDPT (SAL = salicylaldiminate; DPT = dipropylenetriamine), composed of both PCSs and FCSs, could, for instance, be calculated[119] using the ORCA quantum chemistry package[120,121] and the NiSAL-MeDPT structure after refinement at the density functional theory (DFT) level. PCSs were calculated from eqn (5) and the $\Delta\chi$ tensors obtained using state-averaged complete active space self-consistent field (SA-CASSCF),[122] accounting for the dynamic correlations by N-electron valence perturbation theory to the second order (NEVPT2),[123] and FCSs were calculated using the Fermi contact coupling constant and the isotropic g values obtained from DFT calculations. The calculated hyperfine shifts agree very well with the experimental shifts of both complexes (Fig. 9). The accuracy of the calculations allowed for a swap in the assignment of the methylene signals previously reported,[124] and for a refinement of the NiSAL-HDPT structure using the structure of NiSAL-MeDPT as a starting template.[119] The small discrepancies between the calculated shifts and the shifts measured for the HDPT derivative, for which a structure is not experimentally available, were finally rationalized in terms of minor structural changes.

As it is clear from eqn (5), PCSs depend on the magnitude and orientation of the $\Delta\chi$ tensor, which in turn reflects the very fine details of the coordination geometry of the paramagnetic metal ion. For instance, in cobalt(II)-substituted human carbonic anhydrase II, the cobalt(II) ion is essentially tetracoordinated when the enzyme is free in water or bound to sulfonamides, and pentacoordinated in the presence of ligands such as oxalate, where two oxygen atoms of the ligand complete the coordination environment.[125] Indeed, the magnetic susceptibility anisotropy changes dramatically in the two cases.[126]

It was recently figured out that PCSs can be used not only for refining protein structures at the positions of the observed nuclei but also around the paramagnetic center, thus recovering accurate conformational details about the metal ligand positions. In fact, recently, for the first time, it was shown that the paramagnetic $\Delta\chi$ tensor of a large metalloprotein can be calculated *ab initio* with advanced quantum-chemical approaches using only a structural model of the metal coordination site.[33] Using the effective spin Hamiltonian (valid when all orbital excited states are sufficiently more in energy from the ground state with respect to the energy of the thermal bath), the $\Delta\chi$ tensor can also be determined from the $\mathbf{g}$ and the ZFS ($\mathbf{D}$) tensors (see eqn (10)–(12)).[12,23,41,127] From the knowledge of the

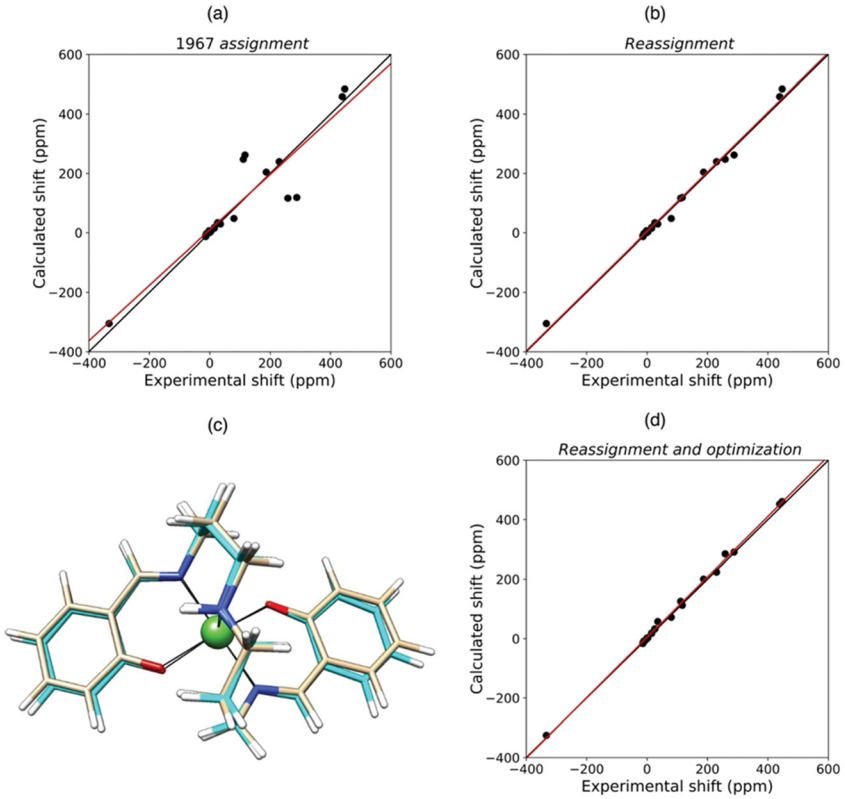

Fig. 9 Agreement between experimental and QC calculated shifts of NiSAL-HDPT, with the assignment previously reported (a),[124] and the theory-based reassignment (b). Comparison between initial (beige) and DFT-optimized (cyan) structures (c) and agreement between the experimental and QC calculated shifts for the refined structure (d).

$\Delta\chi$ tensor and of the protein coordinates, it is easy to predict the PCSs in the point-dipole approximation. A good matching between predicted and experimental PCSs is thus a clear indication of a good prediction of the $\Delta\chi$ tensor.

Conversely, as the magnetic susceptibility tensor is very sensitive to the details of the coordination geometry of the paramagnetic metal ion, the PCSs, measured for nuclei far from the paramagnetic metal, can be used to refine the molecular structure around the metal ion.[82] This approach offers the possibility to overcome one of the most important limitations of paramagnetic NMR, which is the large line broadening often affecting the signals of nuclei in the immediate vicinity of the paramagnetic center, responsible for the presence of a blind sphere. The knowledge of the metal coordination environment at the highest possible resolution is crucial to understand structure–activity relationships for metal ions in proteins and for the successful use of docking strategies for drug discovery.[128,129]

This approach has been tested to refine the structure in solution of the catalytic domain of the human matrix metalloproteinase-12, where the catalytic zinc(II) ion was substituted with the paramagnetic high spin cobalt(II) ion (CoMMP12), coordinated by the *N*-isobutyl-*N*-[4-methoxyphenylsulphonyl]-glycyl hydroxamic acid (NNGH) inhibitor. The cobalt(II) ion coordinates three histidines through their nitrogen atoms, and the inhibitor NNGH through the oxygen atoms of its hydroxamic moiety. A $\Delta\chi$ tensor was obtained using FANTEN[57] from the best fit of the PCS data measured for this protein and the X-ray structure of the NNGH-inhibited zinc(II) protein at 1.34 Å resolution (PDB entry 5LAB[33]), with cobalt(II) replacing zinc(II). The high quality of this fit indicates the good accuracy of the crystallographic model in representing the overall structure of the protein in solution, as well as of the $\Delta\chi$ tensor because it is determined from several hundreds of ^{13}C PCSs.[130] A magnetic susceptibility tensor was also calculated with ORCA[120,121] from the coordinates of the metal ligands taken from the same X-ray structure of the protein. The anisotropy of this QC calculated susceptibility tensor was not found in agreement with the $\Delta\chi$ tensor obtained from the fit of the PCSs. On the other hand, relativistic CASSCF calculations, with second-order perturbation theory corrections, implemented in ORCA, have been shown to be quite reliable in predicting the magnetic properties of transition metal complexes and their temperature dependencies in a number of cases.[119,131,132] Therefore, starting from the crystallographic model of the cobalt(II) coordination cage, a structural refinement procedure was implemented so as to obtain a susceptibility tensor from ORCA in good agreement with the PCSs-derived anisotropy tensor.[133] The structural refinement was performed by adjusting, through a steepest descent search, 19 degrees of freedom among coordination bond lengths, angles and dihedral angles, selected in a way to avoid altering the structure of the ligands themselves. The calculations also showed that an additional proton in the

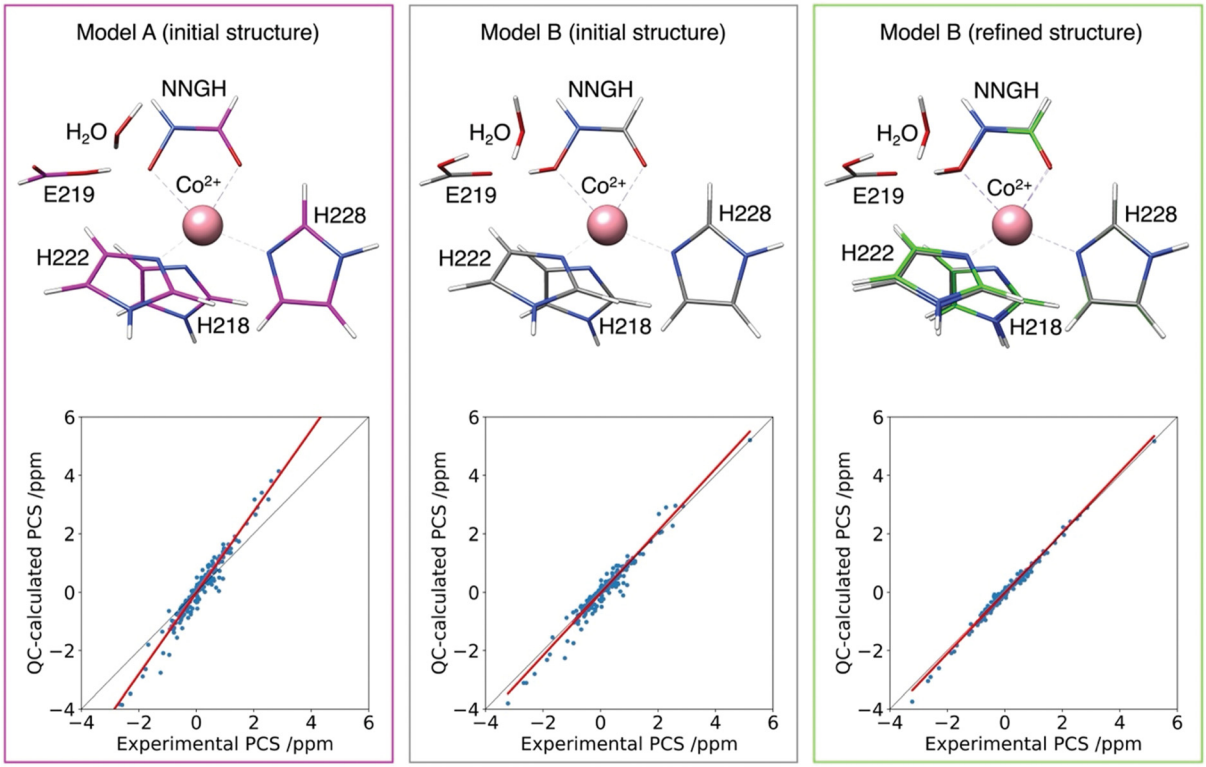

Fig. 10 Agreement between experimental and QC calculated PCSs for the CoMMP-12 protein structure (PDB entry 5LAB) with the hydroxamate (model A initial structure) or the hydroxamic acid moieties of the NNGH inhibitor, before (model B initial structure) and after (model B refined structure) geometry refinement. The refined structure (green) is superimposed to the initial one (grey) to highlight the subtle structural differences.

structure of NNGH should be included (implying that the hydroxamic acid moiety, and not the hydroxamate moiety, coordinates the cobalt(II) ion). This procedure permitted to refine the structure of the metal coordination site in solution to picometer precision (Fig. 10).

In summary, having clarified the QC terms to be included in the hyperfine coupling tensor, and thus having confirmed the dependency of PCSs on the χ tensor from first principles, QC tools can now be used for an accurate prediction of the χ tensor from a structural model of the metal coordination cage, and consequently for an accurate prediction of the PCSs of all protein nuclei from the knowledge of the protein structure, in the point-dipole approximation. The χ tensor can be predicted from relativistic CASSCF/NEVPT2 calculations for metal ions like cobalt(II) and nickel(II). Current challenges are now: (i) to extend the applicability of the QC tools to the robust and efficient prediction of the χ tensor of other paramagnetic metal ions, including lanthanoids(III),[121,134–136] and (ii) to accurately predict PCSs outside the point-dipole approximation.[54]

Also FCSs can be used for the refinement of the metal coordination site to a similar precision. In fact, FCSs depend on the electron spin densities delocalized onto the nuclei, and in turn on the coordination geometry of the paramagnetic metal ion. It has been recently shown that the FCSs measured for ^{1}H, ^{13}C and ^{15}N nuclei of the cobalt(II) ligands in solid-state NMR spectra of the human protein superoxide dismutase 1, in a microcrystalline form and containing a cobalt(II) ion, allowed for the determination of the high-resolution structure of the metal coordination sphere at picometer resolution in the precision of the bond lengths and $\pm1^{\circ}$ resolution of bond angles.[137] A structural model could, in fact, be selected within an ensemble of X-ray structures so as to achieve the best agreement of the measured FCSs with those calculated from the molecular structures using DFT. The structural precision so achieved was enough to correlate the coordination geometry with the unreactive nature of the metal center in these proteins, where it plays a purely structural role.

In perspective, QC calculations of hyperfine shifts are expected to increase in importance and popularity with the increase in computational power, which will extend the applicability of the approach for the structural refinements of proteins even when starting from more distant initial models.

Paramagnetic restraints to monitor protein dynamics

A challenging objective of structural biology is the characterization of the conformational variability which can be exploited by biomolecular systems to perform their biological function. Experimental NMR data are averaged values reflecting this structural variability. Recovering information on the different conformations from these averaged data is a quite cumbersome, ill-posed, inverse problem, which can be tackled in a

number of ways[112,113,138] but always without the possibility of reconstructing a single structural ensemble if *a priori* assumptions are not introduced. In the case of systems composed of multiple structured domains which can reorient with respect to one another, the most used approaches either rely on the Occam's razor[139] (or maximum parsimony) principle or on the maximum entropy principle, aiming at identifying the least populated structural ensembles and the broadest and flattest probability distribution, respectively.[112,113,138] Alternatively, one can rely on unbiased molecular dynamics simulations reweighted in order to achieve an agreement with the experimental data. From a yet different perspective, the maximum occurrence approach[27,28,112,116,138,140] has been proposed to extract the information contained in the averaged data without any prior assumption or calculation. This approach provides the largest weight possible for each allowed conformation, independently from all other conformations present in the ensemble, and is achieved at the cost of giving up the reconstruction of structural ensembles.

Paramagnetic NMR data contain averaged structural information which can be very useful for monitoring the conformational variability of the biomolecular system.[64] For instance, in multidomain proteins, pRDCs are very sensitive to the mobility of a metal-free domain with respect to another domain containing a paramagnetic metal; PREs are very sensitive to even very lowly populated conformations with some nuclei close to the paramagnetic metal, and PCSs are sensitive to both reorientations and translations.

As an example, PCSs and RDCs, complemented by SAXS data, measured for the protein matrix metalloproteinase-1 allowed for the recovery of the mostly populated conformations within the wide structural ensemble experienced by the protein due to the long flexible linker connecting the catalytic and the hemopexin-like domain.[28] These conformations differ largely from the structures obtained by X-ray crystallography.

Conclusions and perspectives

Recent technological advancements, which comprise cryoelectron microscopy and computational methods for structure prediction,[141] offer new tools for the structural characterization of biomolecules, in addition to NMR and X-ray crystallography. Nevertheless, only paramagnetic NMR can offer a spatial resolution on the picometer scale. Therefore, although other techniques can be more advantageous in terms of high-throughput and automation, structural validation and refinement in solution through NMR studies are still crucial for many applications. We thus envision that paramagnetic NMR data, rather than being used for *ab initio* structure calculations, will be increasingly combined with experimental data from different sources in integrative structural biology approaches.

Challenging applications of paramagnetic NMR in structural biology are mainly expected in the following fields:

(1) Refinement of molecular models obtained from other techniques (X-ray crystallography, cryoelectron microscopy, artificial intelligence –AI– predictions). Paramagnetic data offer precious information with an accuracy hardly available using the other techniques and an unprecedented level of detail. Paramagnetic data, in fact, despite their long range nature, provide immediate information about short-range inter-atom distances and bond orientations and can probe the dynamics experienced in solution. Therefore, they are highly suitable to refine conformational models determined using techniques not allowing for such accurate local structural details, and to evaluate the presence of conformational averaging. This approach can improve X-ray structures, which can be affected by structural noise and can be from slightly to significantly inaccurate in solution due to the presence of crystal packing forces, as well as models determined by cryoelectron microscopy and by computational methods for predicting the protein structure, like AlphaFold.[142] Structures determined by cryoelectron microscopy can, in fact, suffer from low resolution, especially in the case of small biomolecules, and can be inaccurate in solution, and the accuracy of AlphaFold structures may need to be improved depending on the required level of structural details.

(2) Evaluation and characterization of the conformational dynamics relevant to functions in systems exploiting structural heterogeneity. In all cases, no or very limited insights into conformational dynamics are obtained using other structural techniques (X-ray crystallography, cryoelectron microscopy, AI predictions). NMR is an irreplaceable technique in this respect, and paramagnetic NMR, in particular, can provide very informative data.

(3) Monitoring of protein–protein interactions and protein–drug interactions in solution. Paramagnetic data can allow for monitoring the presence of interactions between proteins, even if transient and elusive,[116] as well as between proteins and small paramagnetic molecules, even with a low binding affinity. These studies are crucial for the understanding of protein biological functions and for the development of drugs.

(4) Refinement of the metal coordination site of paramagnetic proteins, also taking advantage of the available QC tools. The improvement in QC predictions of paramagnetic NMR data and the development of computational tools for the exploitation of QC data are challenging fields of research. Thanks to QC computations, it can, in fact, be possible to improve the biomolecular structures to a resolution unachievable by any other techniques.[143] Such an accuracy may be needed, for instance, for a thorough understanding of structure–activity relationships and in drug discovery. For a routinary and reliable use of QC tools, much work is still needed for the improvement of the prediction tools, for the whole range of paramagnetic metal ions, in terms of accuracy and computational time, and for cross validation of the predicted data. In parallel, efficient protocols for structural refinement should be implemented. To be noted, the accuracy of X-ray atomic coordinates in the immediate vicinity of a metal ion can sometimes be compromised by phase problems, and AlphaFold is not yet optimized for the structural modeling of metalloproteins.

(5) High magnetic fields represent a challenge not only for relaxation (eqn (2) and (3)) but also because of the span in frequencies that are associated with large hyperfine shifts. Efforts are currently being devoted to the development of pulses that can efficiently cover the full spectral width,[144] as well as for methods that allow for reducing the massive phase distortion that occurs as a result of pulse imperfections and dead time.[145]

(6) When discussing the use of high fields, it is mandatory to mention the use of solid-state NMR, where the absence/reduction of incoherent molecular tumbling yields an effective reduction of the Curie-spin relaxation[146,147] and, in parallel, the appearance of a ''powder pattern'' reflects the geometry and the anisotropy of the interaction of the nuclear spin with the ''Curie Spin'', and encodes highly relevant structural/dynamical information.[11,127,148–150]

The possibility of providing structural information in solution with an increasing level of detail, in conjunction with the possibility of characterizing biomolecular dynamics, is expected to further increase the number of users and applications of paramagnetic NMR, and to foster the development of computational tools and automated protocols for integrated data analysis. These advancements will keep paramagnetic NMR vital in the foreseeable future, contributing to solve challenging and important biological problems.

Conflicts of interest

There are no conflicts to declare.

Acknowledgements

This work has been supported by the Fondazione Cassa di Risparmio di Firenze and the Italian Ministero dell'Istruzione, dell'Università e della Ricerca through the ''Progetto Dipartimenti di Eccellenza 2018–2022'' to the Department of Chemistry ''Ugo Schiff'' of the University of Florence. The authors acknowledge the support and the use of resources of Instruct-ERIC, a landmark ESFRI project, and specifically the CERM/CIRMMP Italy center.

Notes and references

1 E. Luchinat and L. Banci, In-Cell NMR in Human Cells: Direct Protein Expression Allows Structural Studies of Protein Folding and Maturation, *Acc. Chem. Res.*, 2018, **51**, 1550–1557.
2 I. Bertini, M. M. J. Couture, A. Donaire, L. D. Eltis, I. C. Felli, C. Luchinat, M. Piccioli and A. Rosato, The solution structure refinement of the paramagnetic reduced HiPIP I from Ectothiorhodospira halophila by using stable isotope labeling and nuclear relaxation, *Eur. J. Biochem.*, 1996, **241**, 440–452.
3 L. Banci, I. Bertini, K. L. Bren, M. A. Cremonini, H. B. Gray, C. Luchinat and P. Turano, The use of pseudocontact shifts to refine solution structures of paramagnetic metalloproteins: Met80Ala cyano-cytochrome *c* as an example, *J. Biol. Inorg. Chem.*, 1996, **1**, 117–126.
4 L. Banci, I. Bertini, J. G. Huber, C. Luchinat and A. Rosato, Partial orientation of oxidized and reduced cytochrome b5 at high magnetic fields: magnetic susceptibility anisotropy contributions and consequences for protein solution structure determination, *J. Am. Chem. Soc.*, 1998, **120**, 12903–12909.
5 J. R. Tolman, J. M. Flanagan, M. A. Kennedy and J. H. Prestegard, Nuclear magnetic dipole interactions in field-oriented proteins: information for structure determination in solution, *Proc. Natl. Acad. Sci. U. S. A.*, 1995, **92**, 9279–9283.
6 I. Bertini, J. Kowalewski, C. Luchinat and G. Parigi, Cross-correlation between the dipole–dipole interaction and the Curie spin relaxation. The effect of anisotropic magnetic susceptibility, *J. Magn. Reson.*, 2001, **152**, 103–108.
7 I. Bertini, G. Cavallaro, M. Cosenza, R. Kümmerle, C. Luchinat, M. Piccioli and L. Poggi, Cross Correlation Rates Between Curie Spin and Dipole–Dipole relaxation in Paramagnetic Proteins: the Case of Cerium Substituted Calbindin D_{9k}, *J. Biomol. NMR*, 2002, **23**, 115–125.
8 J. C. Hus, D. Marion and M. Blackledge, De novo determination of protein structure by NMR using orientational and long-range order restraints, *J. Mol. Biol.*, 2000, **298**, 927–936.
9 R. Barbieri, C. Luchinat and G. Parigi, Backbone-only protein solution structures with a combination of classical and paramagnetism-based constraints: a method that can be scaled to large molecules, *Chem. Phys. Chem.*, 2004, **21**, 797–806.
10 I. B. Trindade, M. Invernici, F. Cantini, R. O. Louro and M. Piccioli, PRE-driven protein NMR structures: an alternative approach in highly paramagnetic systems, *FEBS J.*, 2021, **288**, 3010–3023.
11 I. Bertini, C. Luchinat, G. Parigi and E. Ravera, *NMR of paramagnetic molecules: applications to metallobiomolecules and models*, Elsevier, 2017.
12 G. Parigi, E. Ravera and C. Luchinat, Magnetic susceptibility and paramagnetism-based NMR, *Prog. Nucl. Magn. Reson. Spectrosc.*, 2019, **114–115**, 211–236.
13 J. S. Griffith, *The theory of transition-metal ions*, Cambridge University Press, Cambridge, 1961, vol. 1.
14 A. Abragam and B. Bleaney, *Electron Paramagnetic Resonance of Transition Metal Ions*, Clarendon Press, Oxford, 1970.
15 I. Solomon, Relaxation Processes in a System of Two Spins, *Phys. Rev.*, 1955, **99**, 559–565.
16 M. Gueron, Nuclear relaxation in macromolecules by paramagnetic ions: a novel mechanism, *J. Magn. Reson.*, 1975, **19**, 58–66.
17 A. J. Vega and D. Fiat, Nuclear relaxation processes of paramagnetic complexes The slow-motion case, *Mol. Phys.*, 1976, **31**, 347–355.
18 E. A. Suturina, K. Mason, C. F. G. C. Geraldes, N. F. Chilton, D. Parker and I. Kuprov, Lanthanide-induced relaxation anisotropy, *Phys. Chem. Chem. Phys.*, 2018, **20**, 17676–17686.

19 I. Bertini, O. Galas, C. Luchinat and G. Parigi, A computer program for the calculation of paramagnetic enhancements of nuclear relaxation rates in slowly rotating systems, *J. Magn. Reson., Ser. A*, 1995, **113**, 151–158.
20 I. Bertini, J. Kowalewski, C. Luchinat, T. Nilsson and G. Parigi, Nuclear spin relaxation in paramagnetic complexes of $S = 1$: electron spin relaxation effects, *J. Chem. Phys.*, 1999, **111**, 5795–5807.
21 J. Kowalewski, D. Kruk and G. Parigi, NMR relaxation in solution of paramagnetic complexes: recent theoretical progress for $S > 1$, *Adv. Inorg. Chem.*, 2005, **57**, 41–104.
22 I. Bertini, C. Luchinat, M. Mancini and G. Spina, The electron-nucleus dipolar coupling. The effect of zero-field splitting of an $S = 3/2$ manifold, *J. Magn. Reson.*, 1984, **59**, 213–222.
23 R. J. Kurland and B. R. McGarvey, Isotropic NMR shifts in transition metal complexes: calculation of the Fermi contact and pseudocontact terms, *J. Magn. Reson.*, 1970, **2**, 286–301.
24 C. Schmitz, R. Vernon, G. Otting, D. Baker and T. Huber, Protein structure determination from pseudocontact shifts using ROSETTA, *J. Mol. Biol.*, 2012, **416**, 668–677.
25 E. A. Suturina and I. Kuprov, Pseudocontact shifts from mobile spin labels, *Phys. Chem. Chem. Phys.*, 2016, **18**, 26412–26422.
26 G. Pintacuda, M. John, X.-C. Su and G. Otting, NMR Structure Determination of Protein−Ligand Complexes by Lanthanide Labeling, *Acc. Chem. Res.*, 2007, **40**, 206–212.
27 L. Gigli, W. Andrałojć, A. Dalaloyan, G. Parigi, E. Ravera, D. Goldfarb and C. Luchinat, Assessing protein conformational landscapes: integration of DEER data in Maximum Occurrence analysis, *Phys. Chem. Chem. Phys.*, 2018, **20**, 27429–27438.
28 L. Cerofolini, G. B. Fields, M. Fragai, C. F. G. C. Geraldes, C. Luchinat, G. Parigi, E. Ravera, D. I. Svergun and J. M. C. Teixeira, Examination of Matrix Metalloproteinase-1 in Solution: A Preference for the Pre-Collagenolysis State, *J. Biol. Chem.*, 2013, **288**, 30659–30671.
29 M. Rinaldelli, E. Ravera, V. Calderone, G. Parigi, G. N. Murshudov and C. Luchinat, Simultaneous use of solution NMR and X-ray data in REFMAC5 for joint refinement/detection of structural differences, *Acta Crystallogr., Sect. D: Biol. Crystallogr.*, 2014, **70**, 958–967.
30 A. Carlon, E. Ravera, W. Andrałojć, G. Parigi, G. N. Murshudov and C. Luchinat, How to tackle protein structural data from solution and solid state: an integrated approach, *Prog. Nucl. Magn. Reson. Spectrosc.*, 2016, **92–93**, 54–70.
31 C. Luchinat, G. Parigi, E. Ravera and M. Rinaldelli, Solid state NMR crystallography through paramagnetic restraints, *J. Am. Chem. Soc.*, 2012, **134**, 5006–5009.
32 B. Bleaney, Nuclear magnetic resonance shifts in solution due to lanthanide ions, *J. Magn. Reson.*, 1972, **8**, 91–100.
33 L. Benda, J. Mareš, E. Ravera, G. Parigi, C. Luchinat, M. Kaupp and J. Vaara, Pseudo-Contact NMR Shifts over the Paramagnetic Metalloprotein CoMMP-12 from First Principles, *Angew. Chem., Int. Ed.*, 2016, **55**, 14713–14717.
34 A. Mondal, M. W. Gaultois, A. J. Pell, M. Iannuzzi, C. P. Grey, J. Hutter and M. Kaupp, Large-Scale Computation of Nuclear Magnetic Resonance Shifts for Paramagnetic Solids Using CP2K, *J. Chem. Theory Comput.*, 2018, **14**, 377–394.
35 J. Mareš and J. Vaara, *Ab initio* paramagnetic NMR shifts *via* point-dipole approximation in a large magnetic-anisotropy Co(II) complex, *Phys. Chem. Chem. Phys.*, 2018, **20**, 22547–22555.
36 J. Chyba, M. Novák, P. Munzarová, J. Novotný and R. Marek, Through-Space Paramagnetic NMR Effects in Host–Guest Complexes: Potential Ruthenium(III) Metallodrugs with Macrocyclic Carriers, *Inorg. Chem.*, 2018, **57**, 8735–8747.
37 P. Srb, M. Svoboda, L. Benda, M. Lepšík, J. Tarábek, V. Šícha, B. Grüner, K. Grantz-Šašková, J. Brynda, P. Řezáčová, J. Konvalinka and V. Veverka, Capturing a dynamically interacting inhibitor by paramagnetic NMR spectroscopy, *Phys. Chem. Chem. Phys.*, 2019, **21**, 5661–5673.
38 A. V. Arbuznikov, J. Vaara and M. Kaupp, Relativistic spin–orbit effects on hyperfine coupling tensors by density-functional theory, *J. Chem. Phys.*, 2004, **120**, 2127–2139.
39 T. O. Pennanen and J. Vaara, Nuclear magnetic resonance chemical shift in an arbitrary electronic spin state, *Phys. Rev. Lett.*, 2008, **100**, 133002.
40 B. Martin and J. Autschbach, Temperature dependence of contact and dipolar NMR chemical shifts in paramagnetic molecules, *J. Chem. Phys.*, 2015, **142**, 054108.
41 A. J. Pell, G. Pintacuda and C. P. Grey, Paramagnetic NMR in solution and the solid state, *Prog. Nucl. Magn. Reson. Spectrosc.*, 2019, **111**, 1–271.
42 J. Vaara, S. A. Rouf and J. Mareš, Magnetic Couplings in the Chemical Shift of Paramagnetic NMR, *J. Chem. Theory Comput.*, 2015, **11**, 4840–4849.
43 B. Martin and J. Autschbach, Kohn–Sham calculations of NMR shifts for paramagnetic 3d metal complexes: protocols, delocalization error, and the curious amide proton shifts of a high-spin iron(II) macrocycle complex, *Phys. Chem. Chem. Phys.*, 2016, **18**, 21051–21068.
44 S. A. Rouf, J. Mareš and J. Vaara, ^{1}H Chemical Shifts in Paramagnetic Co(II) Pyrazolylborate Complexes: A First-Principles Study, *J. Chem. Theory Comput.*, 2015, **11**, 1683–1691.
45 J. Autschbach, *Annual Reports in Computational Chemistry*, Elsevier, 2015, vol. 11, pp. 3–36.
46 J. Autschbach, S. Patchkovskii and B. Pritchard, Calculation of Hyperfine Tensors and Paramagnetic NMR Shifts Using the Relativistic Zeroth-Order Regular Approximation and Density Functional Theory, *J. Chem. Theory Comput.*, 2011, **7**, 2175–2188.
47 P. Hrobárik, R. Reviakine, A. V. Arbuznikov, O. L. Malkina, V. G. Malkin, F. H. Köhler and M. Kaupp, Density functional calculations of NMR shielding tensors for paramagnetic systems with arbitrary spin multiplicity: validation on 3d metallocenes, *J. Chem. Phys.*, 2007, **126**, 024107.
48 T. O. Pennanen and J. Vaara, Density-functional calculations of relativistic spin–orbit effects on nuclear magnetic

shielding in paramagnetic molecules, *J. Chem. Phys.*, 2005, **123**, 174102.
49 G. Parigi, L. Benda, E. Ravera, M. Romanelli and C. Luchinat, Pseudocontact shifts and paramagnetic susceptibility in semiempirical and quantum chemistry theories, *J. Chem. Phys.*, 2019, **150**, 144101.
50 L. Lang, E. Ravera, G. Parigi, C. Luchinat and F. Neese, Solution of a Puzzle: High-Level Quantum-Chemical Treatment of Pseudocontact Chemical Shifts Confirms Classic Semiempirical Theory, *J. Phys. Chem. Lett.*, 2020, **11**, 8735–8744.
51 L. Lang, E. Ravera, G. Parigi, C. Luchinat and F. Neese, Theoretical analysis of the long-distance limit of NMR chemical shieldings, *J. Chem. Phys.*, 2022, **156**, 154115.
52 W. Van den Heuvel and A. Soncini, NMR chemical shift as analytical derivative of the Helmholtz free energy, *J. Chem. Phys.*, 2013, **138**, 054113.
53 L. Cerofolini, J. M. Silva, E. Ravera, M. Romanelli, C. F. G. C. Geraldes, A. L. Macedo, M. Fragai, G. Parigi and C. Luchinat, How Do Nuclei Couple to the Magnetic Moment of a Paramagnetic Center? A New Theory at the Gauntlet of the Experiments, *J. Phys. Chem. Lett.*, 2019, 3610–3614.
54 G. T. P. Charnock and I. Kuprov, A partial differential equation for pseudocontact shift, *Phys. Chem. Chem. Phys.*, 2014, **16**, 20184–20189.
55 I. Bertini, C. Luchinat and G. Parigi, Magnetic susceptibility in paramagnetic NMR, *Prog. Nucl. Magn. Reson. Spectrosc.*, 2002, **40**, 249–273.
56 G. Lipari and A. Szabo, Model-Free approach to the interpretation of nuclear magnetic resonance relaxation in macromolecules. 1. Theory and range of validity, *J. Am. Chem. Soc.*, 1982, **104**, 4546–4559.
57 M. Rinaldelli, A. Carlon, E. Ravera, G. Parigi and C. Luchinat, FANTEN: a new web-based interface for the analysis of magnetic anisotropy-induced NMR data, *J. Biomol. NMR*, 2015, **61**, 21–34.
58 C. Schmitz, M. J. Stanton-Cook, X.-C. Su, G. Otting and T. Huber, Numbat: an interactive software tool for fitting $\Delta\chi$-tensors to molecular coordinates using pseudocontact shifts, *J. Biomol. NMR*, 2008, **41**, 179–189.
59 C. Nitsche and G. Otting, Pseudocontact shifts in biomolecular NMR using paramagnetic metal tags, *Prog. Nucl. Magn. Reson. Spectrosc.*, 2017, **98–99**, 20–49.
60 X.-C. Su and G. Otting, Paramagnetic labelling of proteins and oligonucleotides for NMR, *J. Biomol. NMR*, 2010, **46**, 101–112.
61 D. Joss and D. Häussinger, Design and applications of lanthanide chelating tags for pseudocontact shift NMR spectroscopy with biomacromolecules, *Prog. Nucl. Magn. Reson. Spectrosc.*, 2019, **114–115**, 284–312.
62 P. H. Keizers, J. F. Desreux, M. Overhand and M. Ubbink, Increased paramagnetic effect of a lanthanide protein probe by two-point attachment, *J. Am. Chem. Soc.*, 2007, **129**, 9292–9293.
63 S. Mekkattu Tharayil, M. C. Mahawaththa, C.-T. Loh, I. Adekoya and G. Otting, Phosphoserine for the generation of lanthanide-binding sites on proteins for paramagnetic nuclear magnetic resonance spectroscopy, *Magn. Reson.*, 2021, **2**, 1–13.
64 M. Fragai, C. Luchinat, G. Parigi and E. Ravera, Conformational freedom of metalloproteins revealed by paramagnetism-assisted NMR, *Coord. Chem. Rev.*, 2013, **257**, 2652–2667.
65 D. Parker, E. A. Suturina, I. Kuprov and N. F. Chilton, How the Ligand Field in Lanthanide Coordination Complexes Determines Magnetic Susceptibility Anisotropy, Paramagnetic NMR Shift, and Relaxation Behavior, *Acc. Chem. Res.*, 2020, **53**, 1520–1534.
66 J.-L. Liu, Y.-C. Chen and M.-L. Tong, Symmetry strategies for high performance lanthanide-based single-molecule magnets, *Chem. Soc. Rev.*, 2018, **47**, 2431–2453.
67 J. D. Rinehart and J. R. Long, Exploiting single-ion anisotropy in the design of f-element single-molecule magnets, *Chem. Sci.*, 2011, **2**, 2078–2085.
68 G. Cucinotta, M. Perfetti, J. Luzon, M. Etienne, P.-E. Car, A. Caneschi, G. Calvez, K. Bernot and R. Sessoli, Magnetic Anisotropy in a Dysprosium/DOTA Single-Molecule Magnet: Beyond Simple Magneto-Structural Correlations, *Angew. Chem., Int. Ed.*, 2012, **51**, 1606–1610.
69 N. F. Chilton, D. Collison, E. J. L. McInnes, R. E. P. Winpenny and A. Soncini, An electrostatic model for the determination of magnetic anisotropy in dysprosium complexes, *Nat. Commun.*, 2013, **4**, 2551.
70 F. S. Santana, M. Perfetti, M. Briganti, F. Sacco, G. Poneti, E. Ravera, J. F. Soares and R. Sessoli, A dysprosium single molecule magnet outperforming current pseudocontact shift agents, *Chem. Sci.*, 2022, **13**, 5860–5871.
71 M. P. M. Marques, C. F. G. C. Geraldes, A. D. Sherry, A. E. Merbach, H. Powell, D. Pubanz, S. Aime and M. Botta, NMR conformational study of the lanthanide(III) complexes of DOTA in aqueous solution, *J. Alloys Compd.*, 1995, **225**, 303–307.
72 R. Vogel, T. Müntener and D. Häussinger, Intrinsic anisotropy parameters of a series of lanthanoid complexes deliver new insights into the structure-magnetism relationship, *Chem*, 2021, **7**, 3144–3156.
73 M. Sugita, N. Ishikawa, T. Ishikawa, S. Koshihara and Y. Kaizu, Static Magnetic-Field-Induced Phase Lag in the Magnetization Response of Tris(dipicolinato)lanthanides, *Inorg. Chem.*, 2006, **45**, 1299–1304.
74 B. Bleaney, C. M. Dobson, B. A. Levine, R. B. Martin, R. J. P. Williams and A. V. Xavier, Origin of lanthanide nuclear magnetic resonance shifts and their uses, *J. Chem. Soc., Chem. Commun.*, 1972, 791b–793b.
75 P. H. J. Keizers, A. Saragliadis, Y. Hiruma, M. Overhand and M. Ubbink, Design, Synthesis, and Evaluation of a Lanthanide Chelating Protein Probe: CLaNP-5 Yields Predictable Paramagnetic Effects Independent of Environment, *J. Am. Chem. Soc.*, 2008, **130**, 14802–14812.
76 B. Ma, J.-L. Chen, C.-Y. Cui, F. Yang, Y.-J. Gong and X.-C. Su, Rigid, Highly Reactive and Stable DOTA-like Tags Containing a Thiol-Specific Phenylsulfonyl Pyridine Moiety

for Protein Modification and NMR Analysis**, *Chem. – Eur. J.*, 2021, **27**, 16145–16152.
77 D. Joss, F. Winter and D. Häussinger, A novel, rationally designed lanthanoid chelating tag delivers large paramagnetic structural restraints for biomolecular NMR, *Chem. Commun.*, 2020, **56**, 12861–12864.
78 I. Bertini, K. S. McGreevy and G. Parigi, *NMR in systems biology*, Wiley, 2012.
79 in *Recent developments in biomolecular NMR*, ed. M. Clore and J. Potts, RSC Publ, Cambridge, 2012.
80 V. Gaponenko, S. P. Sarma, A. S. Altieri, D. A. Horita, J. Li and R. A. Byrd, Improving the accuracy of NMR structures of large proteins using pseudocontact shifts as long/range restraints, *J. Biomol. NMR*, 2004, **28**, 205–212.
81 J. Koehler and J. Meiler, Expanding the utility of NMR restraints with paramagnetic compounds: background and practical aspects, *Prog. Nucl. Magn. Reson. Spectrosc.*, 2011, **59**, 360–389.
82 E. Ravera, G. Parigi and C. Luchinat, Perspectives on paramagnetic NMR from a life sciences infrastructure, *J. Magn. Reson.*, 2017, **282**, 154–169.
83 E. Ravera, G. Parigi and C. Luchinat, What are the methodological and theoretical prospects for paramagnetic NMR in structural biology? A glimpse into the crystal ball, *J. Magn. Reson.*, 2019, **306**, 173–179.
84 S. Balayssac, I. Bertini, C. Luchinat, G. Parigi and M. Piccioli, ^{13}C direct detected NMR increases the detectability of residual dipolar couplings, *J. Am. Chem. Soc.*, 2006, **128**, 15042–15043.
85 P. Guentert, Automated NMR structure calculation with CYANA, *Methods Mol. Biol.*, 2004, **278**, 353–378.
86 L. Banci, I. Bertini, G. Cavallaro, A. Giachetti, C. Luchinat and G. Parigi, Paramagnetism-based restraints for Xplor-NIH, *J. Biomol. NMR*, 2004, **28**, 249–261.
87 C. D. Schwieters, J. J. Kuszewski, N. Tjandra and G. Marius Clore, The Xplor-NIH NMR molecular structure determination package, *J. Magn. Reson.*, 2003, **160**, 65–73.
88 I. Bertini, A. Donaire, B. Jimnez, C. Luchinat, G. Parigi, M. Piccioli and L. Poggi, Paramagnetism-based Versus Classical Constraints: An Analysis of the Solution Structure of Ca Ln Calbindin D_{9k}, *J. Biomol. NMR*, 2001, **21**, 85–98.
89 B.-B. Pan, F. Yang, Y. Ye, Q. Wu, C. Li, T. Huber and X.-C. Su, 3D structure determination of a protein in living cells using paramagnetic NMR spectroscopy, *Chem. Commun.*, 2016, **52**, 10237–10240.
90 H. Yagi, K. B. Pilla, A. Maleckis, B. Graham, T. Huber and G. Otting, Three-dimensional protein fold determination from backbone amide pseudocontact shifts generated by lanthanide tags at multiple sites, *Struct. Lond. Engl. 1993*, 2013, **21**, 883–890.
91 K. B. Pilla, J. K. Leman, G. Otting and T. Huber, Capturing Conformational States in Proteins Using Sparse Paramagnetic NMR Data, *PLoS One*, 2015, **10**, e0127053.
92 M. J. Berardi, W. M. Shih, S. C. Harrison and J. J. Chou, Mitochondrial uncoupling protein 2 structure determined by NMR molecular fragment searching, *Nature*, 2011, **476**, 109–113.
93 I. Bertini, A. Bhaumik, G. De Paepe, R. G. Griffin, M. Lelli, J. R. Lewandowski and C. Luchinat, High-Resolution Solid-State NMR Structure of a 17.6 kDa Protein, *J. Am. Chem. Soc.*, 2010, **132**, 1032–1040.
94 A. Bhaumik, C. Luchinat, G. Parigi, E. Ravera and M. Rinaldelli, NMR crystallography on paramagnetic systems: solved and open issues, *CrystEngComm*, 2013, **15**, 8639–8656.
95 I. Bertini, P. Kursula, C. Luchinat, G. Parigi, J. Vahokoski, M. Willmans and J. Yuan, Accurate solution structures of proteins from X-ray data and minimal set of NMR data: calmodulin peptide complexes as examples, *J. Am. Chem. Soc.*, 2009, **131**, 5134–5144.
96 I. de Diego, J. Kuper, N. Bakalova, P. Kursula and M. Wilmanns, Molecular Basis of the Death-Associated Protein Kinase-Calcium/Calmodulin Regulator Complex, *Sci. Signal.*, 2010, **3**, ra6.1–ra6.9.
97 A. Carlon, E. Ravera, G. Parigi, G. N. Murshudov and C. Luchinat, Joint X-ray/NMR structure refinement of multidomain/multisubunit systems, *J. Biomol. NMR*, 2019, **73**, 265–278.
98 W. Andrałojć, C. Luchinat, G. Parigi and E. Ravera, Exploring Regions of Conformational Space Occupied by Two-Domain Proteins, *J. Phys. Chem. B*, 2014, **118**, 10576–10587.
99 M. Zweckstetter and A. Bax, Evaluation of uncertainty in alignment tensors obtained from dipolar couplings, *J. Biomol. NMR*, 2002, **23**, 127–137.
100 A. Schirò, A. Carlon, G. Parigi, G. Murshudov, V. Calderone, E. Ravera and C. Luchinat, On the complementarity of X-ray and NMR data, *J. Struct. Biol.: X*, 2020, **4**, 100019.
101 G. N. Murshudov, P. Skubák, A. A. Lebedev, N. S. Pannu, R. A. Steiner, R. A. Nicholls, M. D. Winn, F. Long and A. A. Vagin, REFMAC5 for the refinement of macromolecular crystal structures, *Acta Crystallogr., Sect. D: Biol. Crystallogr.*, 2011, **67**, 355–367.
102 A. Carlon, E. Ravera, J. Hennig, G. Parigi, M. Sattler and C. Luchinat, Improved Accuracy from Joint X-ray and NMR Refinement of a Protein–RNA Complex Structure, *J. Am. Chem. Soc.*, 2016, **138**, 1601–1610.
103 V. Gaponenko, A. S. Altieri, J. Li and R. A. Byrd, Breaking symmetry in the structure determination of (large) symmetric protein dimers, *J. Biomol. NMR*, 2002, **24**, 143–148.
104 M. Longinetti, G. Parigi and L. Sgheri, Uniqueness and degeneracy in the localization of rigid domains in paramagnetic proteins, *J. Phys. A: Math. Gen.*, 2002, **35**, 8153–8169.
105 W. Andrałojć, K. Berlin, D. Fushman, C. Luchinat, G. Parigi, E. Ravera and L. Sgheri, Information content of long-range NMR data for the characterization of conformational heterogeneity, *J. Biomol. NMR*, 2015, **62**, 353–371.
106 N. J. Anthis, M. Doucleff and G. M. Clore, Transient, Sparsely Populated Compact States of Apo and Calcium-Loaded Calmodulin Probed by Paramagnetic Relaxation Enhancement: Interplay of Conformational Selection and Induced Fit, *J. Am. Chem. Soc.*, 2011, **133**, 18966–18974.

107 M. A. Hass and M. Ubbink, Structure determination of protein–protein complexes with long-range anisotropic paramagnetic NMR restraints, *Curr. Opin. Struct. Biol.*, 2014, **24**, 45–53.
108 E. Ravera, L. Salmon, M. Fragai, G. Parigi, H. Al-Hashimi and C. Luchinat, Insights into Domain–Domain Motions in Proteins and RNA from Solution NMR, *Acc. Chem. Res.*, 2014, **47**, 3118–3126.
109 G. M. Clore, Exploring sparsely populated states of macromolecules by diamagnetic and paramagnetic NMR relaxation, *Protein Sci. Publ. Protein Soc.*, 2011, **20**, 229–246.
110 L. Russo, M. Maestre-Martinez, S. Wolff, S. Becker and C. Griesinger, Interdomain Dynamics Explored by Paramagnetic NMR, *J. Am. Chem. Soc.*, 2013, **135**, 17111–17120.
111 C. Camilloni and M. Vendruscolo, Using Pseudocontact Shifts and Residual Dipolar Couplings as Exact NMR Restraints for the Determination of Protein Structural Ensembles, *Biochemistry*, 2015, **54**, 7470–7476.
112 E. Ravera, L. Sgheri, G. Parigi and C. Luchinat, A critical assessment of methods to recover information from averaged data, *Phys. Chem. Chem. Phys.*, 2016, **18**, 5686–5701.
113 M. Bonomi, G. T. Heller, C. Camilloni and M. Vendruscolo, Principles of protein structural ensemble determination, *Curr. Opin. Struct. Biol.*, 2017, **42**, 106–116.
114 J. Iwahara and G. M. Clore, Detecting transient intermediates in macromolecular binding by paramagnetic NMR, *Nature*, 2006, **440**, 1227–1230.
115 L. Deshmukh, J. M. Louis, R. Ghirlando and G. M. Clore, Transient HIV-1 Gag–protease interactions revealed by paramagnetic NMR suggest origins of compensatory drug resistance mutations, *Proc. Natl. Acad. Sci. U. S. A.*, 2016, **113**, 12456–12461.
116 W. Andrałojć, Y. Hiruma, W.-M. Liu, E. Ravera, M. Nojiri, G. Parigi, C. Luchinat and M. Ubbink, Identification of productive and futile encounters in an electron transfer protein complex, *Proc. Natl. Acad. Sci. U. S. A.*, 2017, **114**, E1840–E1847.
117 J. Schilder, F. Löhr, H. Schwalbe and M. Ubbink, The cytochrome *c* peroxidase and cytochrome *c* encounter complex: the other side of the story, *FEBS Lett.*, 2014, **588**, 1873–1878.
118 S. J. de Vries, M. van Dijk and A. M. Bonvin, The HADDOCK web server for data-driven biomolecular docking, *Nat. Protoc.*, 2010, **5**, 883–897.
119 E. Ravera, L. Gigli, B. Czarniecki, L. Lang, R. Kümmerle, G. Parigi, M. Piccioli, F. Neese and C. Luchinat, A Quantum Chemistry View on Two Archetypical Paramagnetic Pentacoordinate Nickel(II) Complexes Offers a Fresh Look on Their NMR Spectra, *Inorg. Chem.*, 2021, **60**, 2068–2075.
120 F. Neese, The ORCA program system: The ORCA program system, *Wiley Interdiscip. Rev.: Comput. Mol. Sci.*, 2012, **2**, 73–78.
121 F. Neese, Software update: the ORCA program system, version 4.0, *Wiley Interdiscip. Rev.: Comput. Mol. Sci.*, 2018, **8**, e1327.
122 P. E. M. Siegbahn, J. Almlöf, A. Heiberg and B. O. Roos, The complete active space SCF (CASSCF) method in a Newton–Raphson formulation with application to the HNO molecule, *J. Chem. Phys.*, 1981, **74**, 2384–2396.
123 C. Angeli and R. Cimiraglia, Multireference perturbation configuration interaction V. Third-order energy contributions in the Møller–Plesset and Epstein–Nesbet partitions, *Theor. Chem. Acc.*, 2002, **107**, 313–317.
124 G. N. La Mar and L. Sacconi, Proton magnetic resonance studies of high-spin nickel(II) complexes with pentadentate Schiff bases, *J. Am. Chem. Soc.*, 1967, **89**, 2282.
125 I. Bertini and C. Luchinat, Cobalt(II) as a probe of the structure and function of carbonic anhydrase, *Acc. Chem. Res.*, 1983, **16**, 272–279.
126 L. Cerofolini, T. Staderini, S. Giuntini, E. Ravera, M. Fragai, G. Parigi, R. Pierattelli and C. Luchinat, Long-range paramagnetic NMR data can provide a closer look on metal coordination in metalloproteins, *J. Biol. Inorg. Chem.*, 2018, **23**, 71–80.
127 B. J. Walder, A. M. Patterson, J. H. Baltisberger and P. J. Grandinetti, Hydrogen motional disorder in crystalline iron group chloride dihydrates, *J. Chem. Phys.*, 2018, **149**, 084503.
128 I. V. Korendovych and W. F. DeGrado, Catalytic efficiency of designed catalytic proteins, *Curr. Opin. Struct. Biol.*, 2014, **27**, 113–121.
129 S. Signorella, C. Palopoli and G. Ledesma, Rationally designed mimics of antioxidant manganoenzymes: role of structural features in the quest for catalysts with catalase and superoxide dismutase activity, *Coord. Chem. Rev.*, 2018, **365**, 75–102.
130 S. Balayssac, I. Bertini, A. Bhaumik, M. Lelli and C. Luchinat, Paramagnetic shifts in solid-state NMR of proteins to elicit strucutral information, *Proc. Natl. Acad. Sci. U. S. A.*, 2008, **105**, 17284–17289.
131 E. A. Suturina, J. Nehrkorn, J. M. Zadrozny, J. Liu, M. Atanasov, T. Weyhermüller, D. Maganas, S. Hill, A. Schnegg, E. Bill, J. R. Long and F. Neese, Magneto-Structural Correlations in Pseudotetrahedral Forms of the $[Co(SPh)_4]^{2-}$ Complex Probed by Magnetometry, MCD Spectroscopy, Advanced EPR Techniques, and ab Initio Electronic Structure Calculations, *Inorg. Chem.*, 2017, **56**, 3102–3118.
132 P. Kumar, D. J. SantaLucia, K. Kaniewska-Laskowska, S. V. Lindeman, A. Ozarowski, J. Krzystek, M. Ozerov, J. Telser, J. F. Berry and A. T. Fiedler, Probing the Magnetic Anisotropy of Co(II) Complexes Featuring Redox-Active Ligands, *Inorg. Chem.*, 2020, **59**, 16178–16193.
133 E. Ravera, L. Gigli, E. A. Suturina, V. Calderone, M. Fragai, G. Parigi and C. Luchinat, A High-Resolution View of the Coordination Environment in a Paramagnetic Metalloprotein from its Magnetic Properties, *Angew. Chem., Int. Ed.*, 2021, **60**, 14960–14966.
134 M. Atanasov, D. Aravena, E. Suturina, E. Bill, D. Maganas and F. Neese, First principles approach to the electronic structure, magnetic anisotropy and spin relaxation in mononuclear 3d-transition metal single molecule magnets, *Coord. Chem. Rev.*, 2015, **289–290**, 177–214.

135 F. Aquilante, J. Autschbach, R. K. Carlson, L. F. Chibotaru, M. G. Delcey, L. De Vico, I. Fdez Galván, N. Ferré, L. M. Frutos, L. Gagliardi, M. Garavelli, A. Giussani, C. E. Hoyer, G. Li Manni, H. Lischka, D. Ma, P. Å. Malmqvist, T. Müller, A. Nenov, M. Olivucci, T. B. Pedersen, D. Peng, F. Plasser, B. Pritchard, M. Reiher, I. Rivalta, I. Schapiro, J. Segarra-Martí, M. Stenrup, D. G. Truhlar, L. Ungur, A. Valentini, S. Vancoillie, V. Veryazov, V. P. Vysotskiy, O. Weingart, F. Zapata and R. Lindh, Molcas 8: new capabilities for multiconfigurational quantum chemical calculations across the periodic table, *J. Comput. Chem.*, 2016, **37**, 506–541.

136 P. P. Hallmen, H.-J. Werner, D. Kats, S. Lenz, G. Rauhut, H. Stoll and J. van Slageren, Toward fast and accurate ab initio calculation of magnetic exchange in polynuclear lanthanide complexes, *Phys. Chem. Chem. Phys.*, 2019, **21**, 9769–9778.

137 A. Bertarello, L. Benda, K. J. Sanders, A. J. Pell, M. J. Knight, V. Pelmenschikov, L. Gonnelli, I. C. Felli, M. Kaupp, L. Emsley, R. Pierattelli and G. Pintacuda, Picometer Resolution Structure of the Coordination Sphere in the Metal-Binding Site in a Metalloprotein by NMR, *J. Am. Chem. Soc.*, 2020, **142**, 16757–16765.

138 D. M. Selegato, C. Bracco, C. Giannelli, G. Parigi, C. Luchinat, L. Sgheri and E. Ravera, Comparison of Different Reweighting Approaches for the Calculation of Conformational Variability of Macromolecules from Molecular Simulations, *ChemPhysChem*, 2021, **22**, 127–138.

139 G. M. Clore and C. D. Schwieters, How Much Backbone Motion in Ubiquitin Is Required To Account for Dipolar Coupling Data Measured in Multiple Alignment Media as Assessed by Independent Cross-Validation?, *J. Am. Chem. Soc.*, 2004, **126**, 2923–2938.

140 I. Bertini, A. Giachetti, C. Luchinat, G. Parigi, M. V. Petoukhov, R. Pierattelli, E. Ravera and D. I. Svergun, Conformational space of flexible biological macromolecules from average data, *J. Am. Chem. Soc.*, 2010, **132**, 13553–13558.

141 G. Masrati, M. Landau, N. Ben-Tal, A. Lupas, M. Kosloff and J. Kosinski, Integrative Structural Biology in the Era of Accurate Structure Prediction, *J. Mol. Biol.*, 2021, **433**, 167127.

142 J. Jumper, R. Evans, A. Pritzel, T. Green, M. Figurnov, O. Ronneberger, K. Tunyasuvunakool, R. Bates, A. Žídek, A. Potapenko, A. Bridgland, C. Meyer, S. A. A. Kohl, A. J. Ballard, A. Cowie, B. Romera-Paredes, S. Nikolov, R. Jain, J. Adler, T. Back, S. Petersen, D. Reiman, E. Clancy, M. Zielinski, M. Steinegger, M. Pacholska, T. Berghammer, S. Bodenstein, D. Silver, O. Vinyals, A. W. Senior, K. Kavukcuoglu, P. Kohli and D. Hassabis, Highly accurate protein structure prediction with AlphaFold, *Nature*, 2021, **596**, 583–589.

143 G. Parigi, E. Ravera and C. Luchinat, Paramagnetic effects in NMR for protein structures and ensembles: studies of metalloproteins, *Curr. Opin. Struct. Biol.*, 2022, **74**, 102386.

144 S. Asami, W. Kallies, J. C. Günther, M. Stavropoulou, S. J. Glaser and M. Sattler, Ultrashort Broadband Cooperative Pulses for Multidimensional Biomolecular NMR Experiments, *Angew. Chem., Int. Ed.*, 2018, **57**, 14498–14502.

145 E. Ravera, Phase distortion-free paramagnetic NMR spectra, *J. Magn. Reson. Open*, 2021, **8–9**, 100022.

146 G. Kervern, S. Steuernagel, F. Engelke, G. Pintacuda and L. Emsley, Absence of Curie relaxation in paramagnetic solids yields long ^{1}H coherence lifetimes, *J. Am. Chem. Soc.*, 2007, **129**, 14118–14119.

147 L. Gigli, S. Di Grande, E. Ravera, G. Parigi and C. Luchinat, NMR for Single Ion Magnets, *Magnetochemistry*, 2021, **7**, 96.

148 A. Nayeem and J. P. Yesinowski, Calculation of magic-angle spinning nuclear magnetic resonance spectra of paramagnetic solids, *J. Chem. Phys.*, 1988, **89**, 4600–4608.

149 G. Kervern, A. D'Aléo, L. Toupet, O. Maury, L. Emsley and G. Pintacuda, Crystal-Structure Determination of Powdered Paramagnetic Lanthanide Complexes by Proton NMR Spectroscopy, *Angew. Chem., Int. Ed.*, 2009, **48**, 3082–3086.

150 T. Le Marchand, T. Schubeis, M. Bonaccorsi, P. Paluch, D. Lalli, A. J. Pell, L. B. Andreas, K. Jaudzems, J. Stanek and G. Pintacuda, ^{1}H-Detected Biomolecular NMR under Fast Magic-Angle Spinning, *Chem. Rev.*, 2022, **122**, 9943–10018.